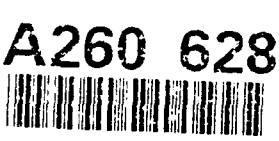

FFA TN 1992-17

FFA TN 1992-17

FLYGTEKNISKA FÖRSÖKSANSTALTEN

The Aeronautical Research Institute of Sweden

RELIABLE STRESS AND FRACTURE MECHANICS ANALYSIS OF COMPLEX AIRCRAFT COMPONENTS USING A h-p VERSION OF FEM

Börje Andersson, Ivo Babuška, Tobias von Petersdorff and Urban Falk

Stockholm 1992

DISCLAIMER NOTICE

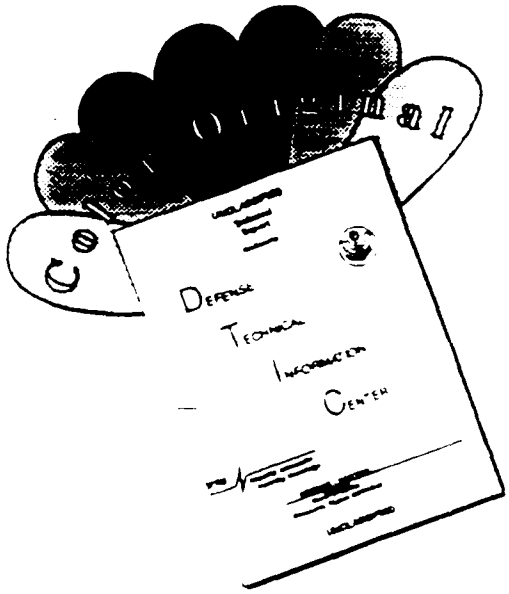

THIS DOCUMENT IS BEST QUALITY AVAILABLE. THE COPY FURNISHED TO DTIC CONTAINED A SIGNIFICANT NUMBER OF COLOR PAGES WHICH DO NOT REPRODUCE LEGIBLY ON BLACK AND WHITE MICROFICHE.

SECURITY CLASSIFICATION OF THIS PAGE (When Data Entered)

REPORT DOCUMENTATION PAGE

READ INSTRUCTIONS BEFORE COMPLETING FORM

1. REPORT NUMBER: FA TN 1992-17	2. GOVT ACCESSION NO.
3. RECIPIENT'S CATALOG NUMBER	
4. TITLE (and Subtitle): Reliable Stress and Fracture Mechanics Analysis of Complex Aircraft Components Using A h-p Version of FEM	5. TYPE OF REPORT & PERIOD COVERED: Final Life of Contract
6. PERFORMING ORG. REPORT NUMBER	
7. AUTHOR(s): Borje Andersson[1] - Ivo Babuska[2]; Tobias von Petersdorff[2] - Urban Falk[1]	8. CONTRACT OR GRANT NUMBER(s): [1]Swedish Defense Material Admin. [2]N00014-9-J-1030 (ONR)
9. PERFORMING ORGANIZATION NAME AND ADDRESS: The Aeronautical Research Institute of Sweden, Structures Department - Box 11021, S-161 11 Bromma, SWEDEN	10. PROGRAM ELEMENT, PROJECT, TASK AREA & WORK UNIT NUMBERS
11. CONTROLLING OFFICE NAME AND ADDRESS: Department of the Navy, Office of Naval Research, Arlington, VA 22217	12. REPORT DATE: August 1992
	13. NUMBER OF PAGES: 50
14. MONITORING AGENCY NAME & ADDRESS(if different from Controlling Office)	15. SECURITY CLASS. (of this report)
	15a. DECLASSIFICATION/DOWNGRADING SCHEDULE

16. DISTRIBUTION STATEMENT (of this Report)

Approved for public release: distribution unlimited

17. DISTRIBUTION STATEMENT (of the abstract entered in Block 20, if different from Report)

18. SUPPLEMENTARY NOTES

19. KEY WORDS (Continue on reverse side if necessary and identify by block number)

20. ABSTRACT

Effective approaches are developed with which complex three-dimensional components may be analyzed with a high and virtually guaranteed accuracy. The main computational tool is a h-p version of FEM practically realized with the p-version program STRIPE having a mesh generator for automatic mesh refinement at edges and vertices. Use of advanced extraction methods and new theoretical approaches give exponential convergence rates for accuracies in all engineering data of interest. New methods for reliable calculation of local stresses and stress intensity data at edges and vertices to be used for fatigue dimensioning at fillets, damage tolerance assessment of three-dimensional flaws etc. are given. A complex real-life problem is reliably analyzed in order to demonstrate the practical usefulness of the procedures advocated. The technical details are given in forthcoming papers.

DD FORM 1 JAN 73 1473 EDITION OF 1 NOV 65 IS OBSOLETE

S/N 0102-LF-014-6601

SECURITY CLASSIFICATION OF THIS PAGE (When Data Entered)

The Aeronautical Research
Institute of Sweden
Structures Department

Reliable Stress and Fracture Mechanics Analysis of Complex Aircraft Components using a h-p Version of FEM

by

Börje Andersson,[1] Ivo Babuška,[2] Tobias von Petersdorff,[2]
and Urban Falk [1]

[1] The Aeronautical Research Institute of Sweden
Box 11021, S-161 11 Bromma, Sweden

[2] Institute for Physical Science and Technology
University of Maryland, College Park, MD 20742, USA

We develop effective approaches with which complex three-dimensional components may be analysed with a high and virtually guaranteed accuracy. The main computational tool is a $h-p$ version of FEM practically realised with the p-version program STRIPE having a mesh generator for automatic mesh refinement at edges and vertices. Use of advanced extraction methods and new theoretical approaches give exponential convergence rates for accuracies in all engineering data of interest. New methods for reliable calculation of local stresses and stress intensity data at edges and vertices to be used for fatigue dimensioning at fillets, damage tolerance assessment of three-dimensional flaws etc. are given. A complex real-life problem is reliably analysed in order to demonstrate the practical usefulness of the procedures advocated. The technical details are given in forthcoming papers.

[1] Research supported by the Swedish Defense Material Administration.
[2] Research partially supported by the US office of Naval Research under the grant N00014-90-J-1030.

Contents

1 INTRODUCTION

Mechanical engineers are faced with the task to design tools which will operate safely under certain mechanical conditions, in certain environments and for certain periods of time. The cost of fabrication and design has to be low and the construction has to meet specific demands on weight and space requirements etc.

Before manufacturing the tool, the designer must be able to predict its behaviour. This prediction is based on a formulation of a mathematical model, its computational analysis, experiments, and experience with existing constructions and their failures. Because of various uncertainties which necessarily occur, the goals of the advanced design analysis (in nuclear industry, aircraft industry etc.) are often stipulated in the design codes (which are changing over time) and are, at least by parts, company oriented. The question of the principles of the safety is directly related to these codes.

For example, in the design code [1] used in military aircraft design, it is required that components based on the principles of "non-inspectable slow crack growth" must be designed under the assumptions that,

a) the as-fabricated structure contains flaws of a size just smaller than the non-destructive maximum undetectable flaw size

b) the flaws are assumed to exist in form of crack-like defects with most unfavourable location and orientation

The design code requires that the mathematical formulation and its computational analysis must reliably and conservatively predict both the sizes of the growing cracks and the residual strength of the component.

Of course an essential part of these principles is nonmathematical as for example the mechanical principles of fatigue crack growth (today mostly based on the phenomenological Paris law or similar laws). For various aspects we refer the reader to [2].

There obviously must be a balance between what can be accurately analyzed and what the design code stipulates. This is influenced by the steady progress of computer hardware as well as progress in the numerical methods. Today and still in the future more and more complex mathematical problems can and will be understood and reliably solved. The role of the effectiveness of the computations, although very important, has to be assessed from this viewpoint, especially when the effectiveness could drastically depend on the computer architecture.

The role of numerical analysis has to be seen also in the light of testing the mathematical models (the formulation) by comparing the computed results with

experiments. Here it is essential that the numerical results are so close to the *exact* solution of the mathematical problem that any observed discrepancy with experimental results is *only* due to the mathematical formulation and not the errors of the numerical analysis. This means that a practical accurate and reliable *a-posteriori* error estimate for *any* data of interest (i.e. not only the usual energy norm estimate) is imperative.

The FE-code has to be adaptive in the sense that given a tolerance for the error in stress, stress intensity factor etc. the FE-code automatically increases the accuracy until the error becomes lower than requested by the user. The increase in accuracy of a FE-solution may be obtained in basically three different ways.

a) The h-version. Here the degrees of the elements are fixed and the program adaptively refines the mesh (uniformly or non-uniformly) until the desired accuracy is achieved. There are several h-adaptive codes. We refer to [3],[4] as examples

b) The p-version. Here the mesh is fixed and the element degrees p are adaptively increased (possibly non-uniformly) until the desired accuracy is achieved. The programs MSC/PROBE (McNeal Schwendler Corp.), STRIPE (The Aeronautical Research Institute of Sweden), Applied Structure (Rasna Corp.) belong to this category. Although in principle, the method gives the result needed for any mesh, practically the mesh is of utmost importance.

c) The $h-p$ version. Here the code adaptively refines the mesh and selects the degrees p. The code PHLEX (Computational Mechanics Corp., Austin) utilizes the $h-p$ version of FEM

If the p-version is used on a properly designed mesh it essentially produces the accuracy of the $h-p$ version. By following simple rules for mesh design one almost achieves the exponential convergence rate for accuracies of interest. In what will follow, we concentrate on the p-version of FEM which combined with properly graded meshes gives a convergence rate similar to that of the $h-p$ version.

One of the major advantages of the p-version is that in sequential computations for increasing p a sequence of solutions for the parameter of interest is obtained from which one can make very reliable assessments of the accuracy of the solution. In principle this can be done for the h-version too, although for practical three-dimensional problems the number of degrees of freedom quickly become prohibitively high.

In this and forthcoming papers we will especially concentrate on problems which are relevant to the criteria of fatigue crack initiation and stable crack growth of flaws in metallic structures.

The mathematical model considered is the Navier-Lamé equations of three-dimensional linear elasticity. We will address the mathematical models and the numerical procedures and give practical examples of the achievements. We will concentrate here on the cases where the mathematical model is given in a deterministic way. To make our ideas as clear as possible we will analyze an academic example and a complex fuselage part.

In section 2 we will discuss a three-dimensional elasticity model problem. We concentrate on its solution in a neighbourhood of the edges and vertices. The singular behaviour of the solution in these neighbourhoods is characterized by *edge* stress intensity functions and *vertex* stress intensity factors. We show that the *p*-version on a proper mesh together with use of extraction procedures leads to accurate computations of these functions and factors as well as stresses with virtually guaranteed *a-posteriori* error estimation. We also show that the stress intensity functions and factors converge with the same rate as the energy error of the finite element solution (i.e. as the square of the energy norm) and that the convergence is exponential in the accuracy range of practical interest.

In the section 3 we adress the problem of reliable *stress calculation* in complex three-dimensional components. A complex fuselage frame is analyzed with the fatigue design problem in mind. An effective method for the design of the radices at fillets is described. We concentrate on the reliability of the computed data and the *a-posteriori* error estimation in the context of the analysis of the fuselage frame problem. Section 4 discusses the *damage tolerance analysis* of complex three-dimensional components. The fuselage component frame with cracks of different sizes is analyzed. Section 5 adresses the computational aspects of the $h-p$ version. It describes the essential parts of the computations and presents basic information about Cpu-times and memory needed. The sizes of the problems are 60000 to 1260000 degrees of freedom.

Section 6 summarices the basic properties of the $h-p$ version, its relibably error estimation and practical experience. All data and experience is based on the use of the program STRIPE developed at the Aeronautical Research Institute of Sweden.

The computational methods presented here are very well covered by a mathematical theory. In the following papers [5], [6],[7],[8],[9],[10] we will elaborate in detail on these methods and their computational aspects.

2 A MODEL PROBLEM AND ITS ANALYSIS

In order to exemplify the character of the solutions to problems in three-dimensional elastomechanics, we consider the folded plate Ω shown in figure 1. The plate is loaded with parabolic sh. .r in the symmetry section.

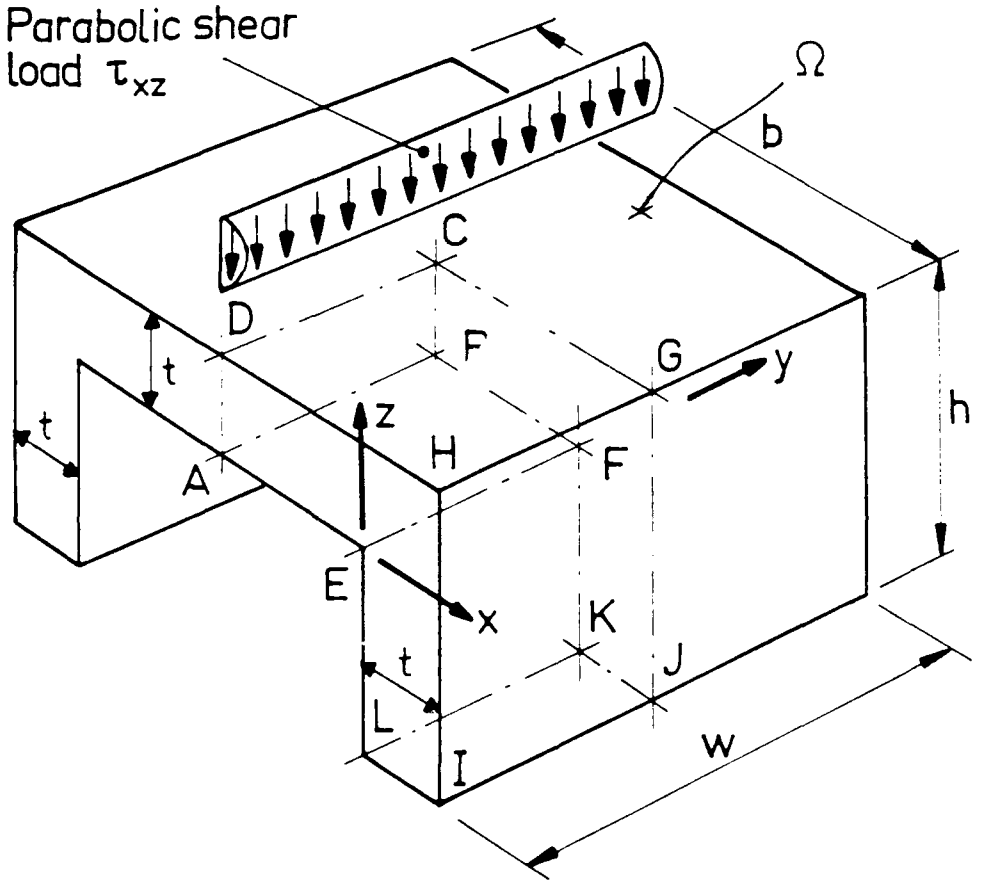

Figure 1: Folded plate loaded with parabolic shear in symmetry section. Plate is clamped to a rigid foundation (the plane $z = t - h$)

Because of symmetry only 1/4'th of the domain is analyzed. Material properties are assumed isotropic and linearly elastic. The modulus of elasticity is denoted E and Poisson's ratio ν. Cartesian displacements and stresses are denoted u, v, w and $\sigma_x, \sigma_y, \sigma_z$, τ_{xy}, τ_{xz} and τ_{yz} respectively.

The face $ABCD$ is loaded by the parabolic tangential shear,

$$\begin{aligned} \tau_{xz} &= 4(z/t)(1-z/t) \\ \tau_{xy} &= 0 \end{aligned} \tag{1}$$

where t is the thickness.

The x-displacements are u=0 on the face $ABCD$. The face $IJKL$ is clamped i.e.

$$u = v = w = 0 \tag{2}$$

On the face $BFKJGC$ the symmetry conditions are,

$$\begin{aligned} v &= 0 \\ \tau_{yz} &= 0 \\ \tau_{xy} &= 0 \end{aligned} \tag{3}$$

All other faces are traction free.

This problem was analyzed as a benchmark problem in [11] and [12]. It is an excellent academic benchmark problem illuminating the difficulties of reliable computations. We will address here the dependence of $\sigma_x(x,0,0)$ on Poisson's ratio ν and the behaviour of the solution close to the vertex E and the edge EF.

Let us list the major theoretical properties of the solution to this mathematical problem.

- There exists exactly one solution which has finite energy
- The solution is analytic everywhere on Ω and its faces except for the edges. Because of symmetry the solution is also analytic on the edge $JGCBFK$
- The solution is singular along edges and the vertices

In a neighbourhood of the edges and the vertices the solution can be written as a sum of singular terms and a smoother function. The singular behaviour is different.

- along the open edges
- in a neighbourhood of the vertices

2.1 Solution behaviour close to edges

We will discuss the properties of the exact solution close to the edge EF.

Denoting by r the distance of the point (x, y, z) from edge EF and by θ ($0 \leq \theta \leq 3\pi/2$) the polar angle, the displacements have, for any $s \geq 1$ and $s \neq Re[\lambda_\alpha^{(j)}]$, the form [13]

$$\begin{bmatrix} u(r,\theta,y) \\ v(r,\theta,y) \\ w(r,\theta,y) \end{bmatrix} = \sum_{Re[\lambda_I^{(j)}]+k \leq s} K_I^{(j,k)}(y) r^{\lambda_I^{(j)}+k} \Psi_I^{(j,k)}(\theta) + \sum_{Re[\lambda_{II}^{(j)}]+k \leq s} K_{II}^{(j,k)}(y) r^{\lambda_{II}^{(j)}+k} \Psi_{II}^{(j,k)}(\theta) + \sum_{Re[\lambda_{III}^{(j)}]+k \leq s} K_{III}^{(j,k)}(y) r^{\lambda_{III}^{(j)}+k} \Psi_{III}^{(j,k)}(\theta) + \text{smoother term} \quad (4)$$

where for k zero or even $\Psi_\alpha^{(j,k)}$ ($\alpha = I$, II or III in the following) are of the form

$$\Psi_I^{(j,k)}(\theta) = \begin{bmatrix} \Phi_{I,1}^{(j,k)}(\theta) \\ 0 \\ \Phi_{I,3}^{(j,k)}(\theta) \end{bmatrix}, \quad \Psi_{II}^{(j,k)}(\theta) = \begin{bmatrix} \Phi_{II,1}^{(j,k)}(\theta) \\ 0 \\ \Phi_{II,3}^{(j,k)}(\theta) \end{bmatrix}, \quad \Psi_{III}^{(j,k)}(\theta) = \begin{bmatrix} 0 \\ \Phi_{III,2}^{(j,k)}(\theta) \\ 0 \end{bmatrix}$$

and for k odd

$$\Psi_I^{(j,k)}(\theta) = \begin{bmatrix} 0 \\ \Phi_{I,2}^{(j,k)}(\theta) \\ 0 \end{bmatrix}, \quad \Psi_{II}^{(j,k)}(\theta) = \begin{bmatrix} 0 \\ \Phi_{II,2}^{(j,k)}(\theta) \\ 0 \end{bmatrix}, \quad \Psi_{III}^{(j,k)}(\theta) = \begin{bmatrix} \Phi_{III,1}^{(j,k)}(\theta) \\ 0 \\ \Phi_{III,3}^{(j,k)}(\theta) \end{bmatrix}$$

The edge intensity functions $K_\alpha^{(j,k)}(y)$ for $k > 0$ can be expressed as a linear combination of derivatives of $K_\alpha^{(j,0)}(y)$. In the sequel we will use the notation $K_\alpha^{(j)}(y) = K_\alpha^{(j,0)}(y)$. In technical applications $K_I^{(1)}(y)$, $K_{II}^{(1)}(y)$ and $K_{III}^{(1)}(y)$ are the important edge intensity functions.

Here functions $\Phi_{\alpha,m}^{(j,k)}$ depend only on local geometry, material and local boundary conditions. In fact the functions

$$r^{\lambda_I^{(j)}} \begin{bmatrix} \Phi_{I,1}^{(j,0)}(\theta) \\ 0 \\ \Phi_{I,3}^{(j,0)}(\theta) \end{bmatrix}, \quad r^{\lambda_{II}^{(j)}} \begin{bmatrix} \Phi_{II,1}^{(j,0)}(\theta) \\ 0 \\ \Phi_{II,3}^{(j,0)}(\theta) \end{bmatrix}$$

are identical with the singular functions for two-dimensional elasticity and the functions

$$r^{\lambda_{III}^{(j)}} \begin{bmatrix} 0 \\ \Phi_{III,2}^{(j,0)}(\theta) \\ 0 \end{bmatrix}$$

are the singular functions for the torsion problem, i.e. the Laplace operator.

Edge stress intensity functions $K_I^{(j)}(y)$, $K_{II}^{(j)}(y)$ and $K_{III}^{(j)}(y)$ are analytic on the semi-open interval $0 < y \leq w/2$, singular at y=0 and depend on the global data of the problem.

The values $\lambda_\alpha^{(j)}$ can also be complex. In this case the functions $\Phi_{I,1}^{(j)}$, $\Phi_{I,3}^{(j)}$ are complex too and the real part of (4) is taken instead. In this case the solution has an oscillatory character. In general, for exceptional cases (geometrical angles or material data), besides the term r^λ there can also be terms of the form $r^\lambda(\log r)^q$ (we will not address this case here).

In (4) we assume that the singularity exponents are numbered such that $Re[\lambda_\alpha^{(j)}] \leq Re[\lambda_\alpha^{(j+1)}]$. The stresses are infinite if any $Re[\lambda_\alpha^{(j)}] < 1$ and the corresponding edge intensity function is nonzero.

$\lambda_I^{(1)}$	$\lambda_I^{(2)}, \lambda_I^{(3)}$	$\lambda_{II}^{(1)}$	$\lambda_{II}^{(2)}, \lambda_{II}^{(3)}$
0.544	$1.629 \pm 0.231i$	0.909	$2.391 \pm 0.316i$

Table 1: First edge eigenvalues $\lambda_I^{(j)}$ and $\lambda_{II}^{(j)}$ for edge EF

$\lambda_{III}^{(1)}$	$\lambda_{III}^{(2)}$	$\lambda_{III}^{(3)}$
0.667	1.333	2

Table 2: First edge eigenvalues $\lambda_{III}^{(j)}$ for edge EF

For the model example the first edge eigenvalues $\lambda_\alpha^{(j)}$ are given in tables 1 and 2. These values, which are independent of Poisson's ratio ν, are obtained by solving a nonlinear equation [14],[15]. We see that the first term for the mode I, mode II and mode III components of (4) yield infinite stresses at the edge EF.

The edge stress intensity function $K_I^{(j)}(y)$ has in a neighbourhood of y=0 the following form

$$K_I^{(j)}(y) = \sum_{l=1}^{L} s_{I,l}^{(j)} y^{\gamma_{I,l}^{(j)}} + \text{smoother term} \tag{5}$$

The intensity factor $s_{I,l}^{(j)}$ is the mode I *vertex-edge* intensity factor of order j for edge EF at vertex E. The exponent $\gamma_{I,l}^{(j)}$ is related to the values of $\lambda_I^{(j)}$ and $\Lambda_1^{(l)}$ characterizing the edge and the vertex singularities as discussed below. Analogous expressions apply for the mode II and mode III edge stress intensity functions.

2.2 Solution behaviour close to vertices

In a neighbourhood of the vertices E, L and I the solution has a singular behaviour which in spherical coordinates can be expressed as

$$\begin{bmatrix} u(r,\omega,\phi) \\ v(r,\omega,\phi) \\ w(r,\omega,\phi) \end{bmatrix} = \sum_{j=1}^{J} S^{(j)} r^{\Lambda^{(j)}} \begin{bmatrix} \Theta_1^{(j)}(\omega,\phi) \\ \Theta_2^{(j)}(\omega,\phi) \\ \Theta_3^{(j)}(\omega,\phi) \end{bmatrix} + \text{smoother terms} \qquad (6)$$

In (6) the coefficients $S^{(j)}$ are the *vertex* intensity factors. The functions Θ_i can be understood to be defined on the intersection of the domain and a spherical surface. This intersection has a boundary with the corners (ω_k, ϕ_k) associated to the edge k of the domain.

For angle (ω_k, ϕ_k) associated with edge EF and for $\nu > 0$ the functions $\Theta_i^{(1)}, \Theta_i^{(4)}, \Theta_i^{(5)}$, (with $i = 1,2,3$) are found (in the numerical analysis) to correspond to a pure mode I deformation at the edge EF. The functions $\Theta_i^{(2)}$ and $\Theta_i^{(3)}$ correspond to a *combined* mode II and mode III deformation of EF with a zero mode I component.

ν	$\Lambda^{(1)}$	$\Lambda^{(2)}$	$\Lambda^{(3)}$	$\Lambda^{(4-5)}$
0.0	0.544	0.909	1.054	1.629
0.30	0.625	0.785	1.237	$1.521 \pm 0.172i$
0.45	0.711	0.751	1.316	1.331

Table 3: The vertex coefficients $\Lambda^{(j)}$ for vertex E

For vertex E the first vertex singularity exponents $\Lambda^{(j)}$ are given in table 3. By comparing (4) and (6) we get the coefficients $\gamma_{I,l}^{(j)}$ in (5) as

$$\gamma_{I,l}^{(j)} = \Lambda^{(j)} - \lambda_I^{(j)}. \qquad (7)$$

In (7) we consider only l-values which are associated with a mode I deformation of edge EF (*e.g.* $l = 1,4,5,\ldots$).

	$l=1$	$l=2$	$l=3$	$l=4$ and $l=5$
$\gamma_{I,l}^{(j)}$	0.081	-	-	$0.977 \pm 0.172i$
$\gamma_{II,l}^{(j)}$	-	-0.123	0.329	-
$\gamma_{III,l}^{(j)}$	-	0.119	0.571	-

Table 4: The coefficients $\gamma_{I,l}^{(j)}$, $\gamma_{II,l}^{(j)}$ and $\gamma_{III,l}^{(j)}$ for edge EF at vertex E for the case ν=0.3

In table 4 the first coefficients are given for the case $\nu = 0.3$.

We see that edge stress intensity functions can be bounded, go to zero or can be unbounded for y small. We mention that in our example some $s_{I,l}^{(j)}$ in (5) could be zero. In fact this occurs in the case $\nu = 0$ because the solution is y-independent.

On the edge AE in a neighbourhood of the vertex E we get, using (6), the stress

$$\sigma_x = \sum_{l=1}^{J} q_l(-x/t)^{\lambda^{(l)}-1} + \text{smoother term.} \tag{8}$$

The stress σ_x is singular at vertex E for all values ν provided that the coefficients $q_1 \neq 0$ or $q_2 \neq 0$. As we will see later for particular values of ν, some coefficients q_l could be zero (especially q_1) and hence it is essential that two terms in (6) and (8) are determined.

We have briefly described the properties of the exact problem to our benchmark problem. For a theoretical discussion of the convergence properties of the p-version in three dimensions, see ([16],[17]).

The characterization of the three-dimensional solution is of great importance since the properties of the exact solution influence drastically the performance of the finite element method and have direct impact on the proper design of the mesh. Let us note that for the design of a mesh we do not have to know the exact character of the singularities. In fact we normally do not know them. We nevertheless know the qualitative character of these singularities and we can design a good mesh following simple *a-priori* known rules. The mesh which, if optimal, should be refined (cylindrically) in a neighbourhood of edges and in a neighbourhood of the vertices (spherically).

Let us now discuss some numerical results for the following model dimensions.

$$\begin{aligned} b/t &= 300 \\ h/t &= 50 \\ w/t &= 100 \\ t &= 100 \end{aligned} \tag{9}$$

We will present results computed by the finite element program STRIPE based on a p-version of the finite element method. Results obtained with the h-version of FEM are given in [11].

In figure 2 we show the mesh used for the computation. In a neighbourhood of the edge EF and the vertex E we used a strongly refined mesh as shown. The mesh used has three spherical layers of elements around vertex E and six cylindrical layers of elements around edge EF. Using this mesh in combination with the p-version of FEM, reliable results will be obtained. The mesh used has 262 elements.

In table 5 we report the energy $\|\tilde{u}\|^2_{E(\Omega)}$ of the finite element solution as a function of p and ν and the relative error $\|e\|^2_{E(\Omega)} = \|u - \tilde{u}\|^2_{E(\Omega)}$ in the energy (the exact

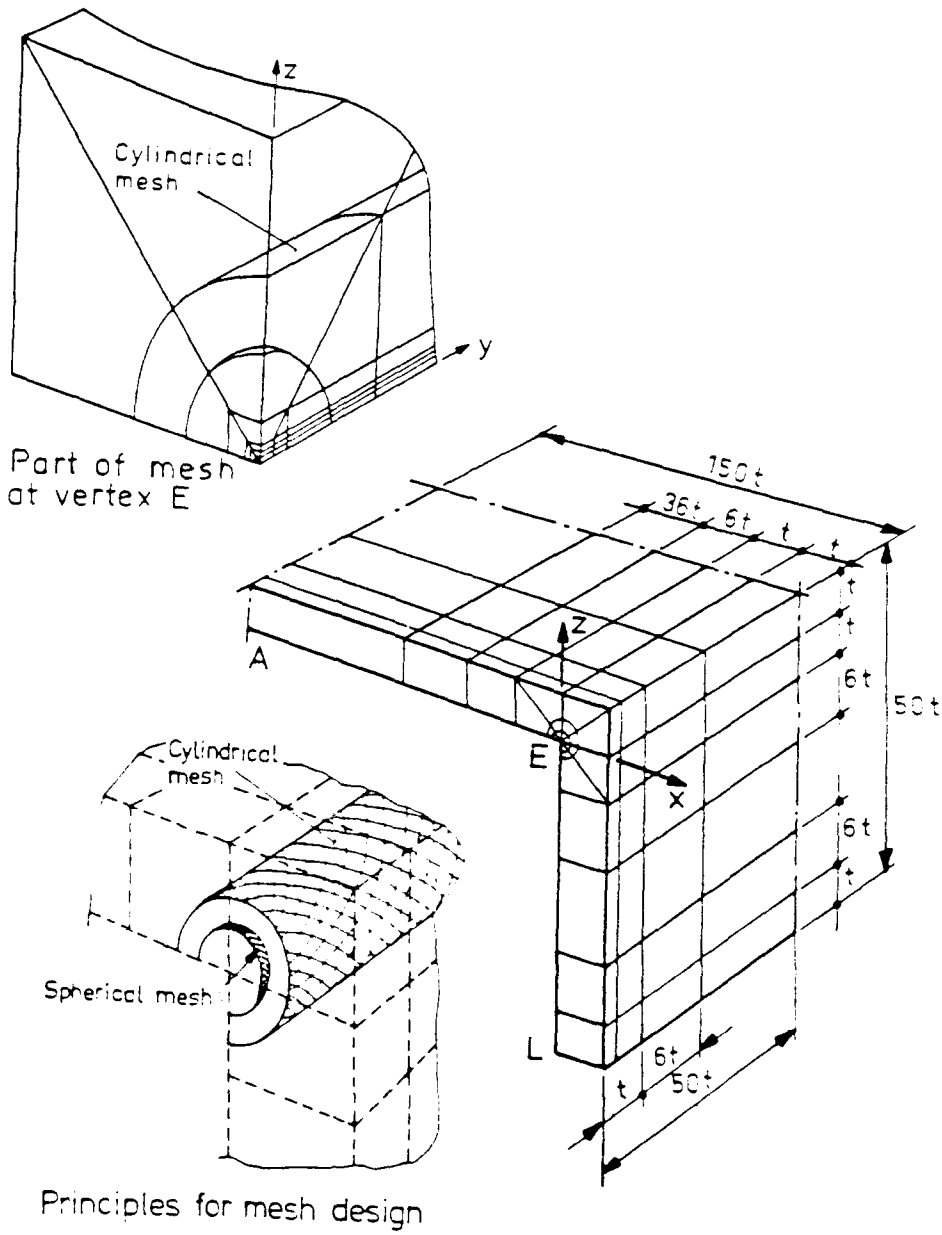

Figure 2: Mesh used for analysis of benchmark problem

	$\nu = 0$		$\nu = 0.30$		$\nu = 0.45$	
p	$\|\|\tilde{u}\|\|^2_{E(\Omega)}$	$\|\|\epsilon\|\|^2_{E(\Omega)}$	$\|\|\tilde{u}\|\|^2_{E(\Omega)}$	$\|\|\epsilon\|\|^2_{E(\Omega)}$	$\|\|\tilde{u}\|\|^2_{E(\Omega)}$	$\|\|\epsilon\|\|^2_{E(\Omega)}$
2	5.600008	3.500017	4.959967	3.680763	3.480780	4.584843
3	9.054089	0.045936	8.414659	0.226071	7.563369	0.502254
4	9.098895	0.001130	8.600359	0.040371	7.961862	0.103761
5	9.099861	0.000164	8.638234	0.002496	8.058791	0.006832
6	9.099963	0.000062	8.639845	0.000885	8.063074	0.002549
7	9.099999	0.000026	8.640380	0.000350	8.064567	0.001056
Estim.	9.100025		8.640730		8.065623	

Table 5: The energy $\|\tilde{u}\|^2_{E(\Omega)}$ and the energy error of the FE-solution $\|\epsilon\|^2_{E(\Omega)}$ obtained with the 262 element mesh. Data given are scaled with a factor 10^{-13}

energy was estimated by extrapolation). We see that the p-version provides a very good assessment of the accuracy achieved and that the accuracy is influenced by the Poisson ratio ν.

Let us note that the convergence with respect to p has two phases. The first one (preasymptotic) has exponential convergence rate while the second has algebraic convergence rate. The reason is that for high p the mesh is "underrefined" and that the rate is algebraic (see [18] and [19]) because the governing error resides in the elements which contains the edges and vertices. The transition between the two phases occurs roughly when errors in these elements becomes the dominating part. The design of the mesh is near optimal when the required accuracy is achieved at the end of the transition part.

In general some overrefinement is recommended because we would like to avoid having an algebraic rate of convergence. The mesh in a neighbourhood of the singularity is recommended to be geometric with the ratio 0.15. This ratio is in some sence optimal. For a theoretical analysis of the one-dimensional model which is roughly applicable here, see [20],[21].

Figure 3 shows in a lin-log scale the stress $\sigma_x(x,0,0)$ and $\sigma_x(x,w/2,0)$ for various values of the Poisson ratio ν. Stresses have been obtained by direct calculation from the displacements. For x very small there is a considerable jump in computed stresses at element boundaries. We see that at the edge AE the stress distribution is very different from the stress at the line $(x,w/2,0)$. For $\nu = 0$ there is no difference between these behaviours. Close to vertex E, we see the strong influence of Poisson's ratio on the stress σ_x .

Table 6 to Table 8 shows the coefficients q_1 and q_2 and vertex exponents $\Lambda^{(1)}$ and $\Lambda^{(2)}$ computed ([8],[22]) using the mesh shown in figur . The coefficients q_i have been obtained from computed Λ-values and eigenfunctions $\Theta_i^{(j)}$ (see (6)).

Values labelled "exact" in table 6 have been obtained with a very detailed two-dimensional model and p=10 uniformly. All digits of the "exact" values are believed

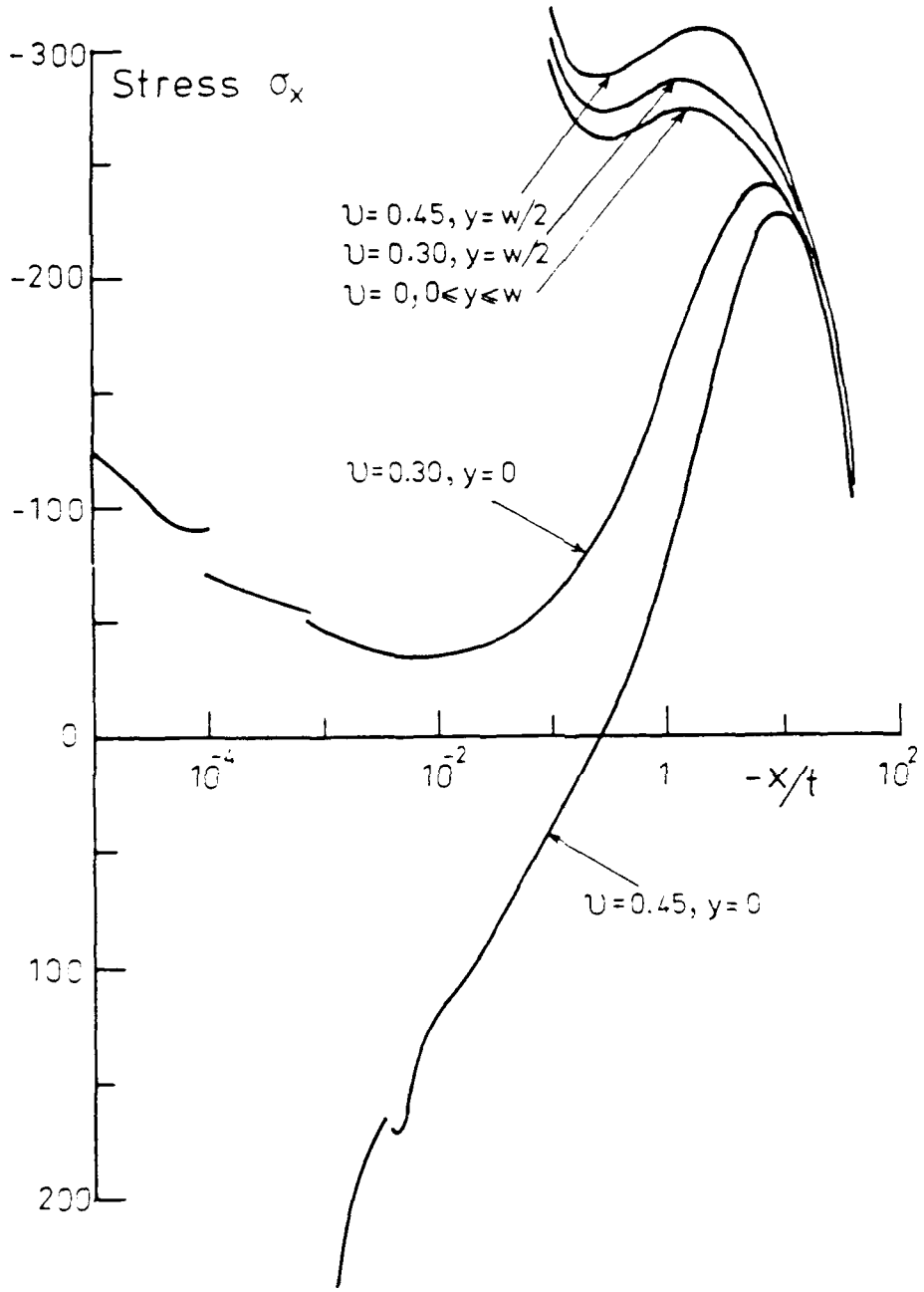

Figure 3: Calculated stress distributions $\sigma_x(x,0,0)$ and $\sigma_x(x,w/2,0)$ for benchmark problem ($p = 7$ solution)

p	$\Lambda^{(1)}$	$\Lambda^{(2)}$	q_1	q_2
3	0.5442	0.9079	-73.06	14.67
4	0.5444	0.9080	-75.24	6.11
5	0.5445	0.9085	-75.81	-1.39
6	0.5445	0.9085	-75.87	-1.55
7	0.5445	0.9085	-75.87	-1.61
Exact	0.5445	0.9085	-75.89	-1.61

Table 6: Calculated Λ-values and q-values as function of p for $\nu = 0$

p	$\Lambda^{(1)}$	$\Lambda^{(2)}$	q_1	q_2
3	0.6256	0.7871	-10.74	-1.10
4	0.6254	0.7853	0.06	-9.77
5	0.6253	0.7851	-1.13	-9.01
6	0.6253	0.7852	-0.45	-8.70
7	0.6253	0.7852	-0.22	-8.68

Table 7: Calculated Λ-values and q-values as function of p for $\nu = 0.30$

p	$\Lambda^{(1)}$	$\Lambda^{(2)}$	q_1	q_2
3	0.7115	0.7548	26.51	-2.70
4	0.7118	0.7514	44.43	-11.90
5	0.7116	0.7510	42.45	-10.35
6	0.7116	0.7511	43.54	-9.84
7	0.7116	0.7511	43.80	-9.84

Table 8: Calculated Λ-values and q-values as function of p for $\nu = 0.45$

to be significant.

We see that

a) the accuracy of computed data can be judged from the sequence of solutions generated

b) the coefficients Λ and q can be accurately computed (except for q_1 when $\nu = 0.3$)

c) for $\nu = 0.3$ the first *vertex* intensity factor $S^{(1)}$ occasionally is very small leading to a very small region with high stresses (compare figure 3)

d) for $\nu > 0.3$ we have the *paradoxical* result that for x small the stress σ_x is infinite with sign opposite to what one would expect

Figure 4 show the energy error $\|e\|^2_{E(\Omega)}$, the error in values $\Lambda^{(1)}$, $\Lambda^{(2)}$, and q_1 for the case ν=0. We see that the error in $\Lambda^{(1)}$ and in q_1 has same character as the accuracy of the energy.

In figure 5 we show in lin-log scale the graph of the function $\sigma_x(x, 0, 0)$ as function of x for various Poisson's ratios when computed from the asymptotic expansion (8) using the first 7 terms. The asymptotic expansions are in good agreement with stresses calculated directly from the FE-solution with $p = 7$.

Let us now address the stresses at the edge EF. Here stresses are infinite and we have to compute the edge stress intensity functions $K_I^{(j)}(y)$, $K_{II}^{(j)}(y)$ and $K_{III}^{(j)}(y)$. In a forthcoming paper [10] we will describe the procedure used. Briefly, the intensity functions are approximated by piecewise polynomials (or trigonometric functions) as

$$K_I^{(j)}(y) \approx \sum_{i=0}^{p} c_i Q_i(y) \tag{10}$$

where $Q_i(y)$ is the Legendre polynomial of order i and c_i are coefficients to be calculated. We compute the coefficients c_i when EF is divided into the three sub-intervals $0 < y < t, t < y < 7t$, $7t < y < 50t$ (compare figure 2).

In table 9 we show the calculated values of $K_I^{(1)}(y)$ (from (10)) in the three mentioned intervals for $\nu = 0.3$ as function of p. Further, $K_I^{(1)}(0)$ is found to be close to zero as predicted from (5) and table 4. For higher values of p the *calculated* intensity function $K_I^{(1)}(y)$ is continuous over the interval $0 \le y \le w/2$.

In figure 6 we show in log-log scale the function $K_I^{(1)}(y)$ (the $p = 8$-solution) for ν=0.3 and x small. Since q_1 is almost zero (table 7) we expect that the second term in (5) influencing $K_I^{(1)}(y)$ might be the dominating one (except for y very small). Figure 6 reveals that this is the case. Note that because $\gamma_{I,4}^{(0)}$ and $\gamma_{I,5}^{(0)}$ are complex $K_I^{(1)}(y)$ is oscillatory but only in a close neighbourhood of $y = 0$.

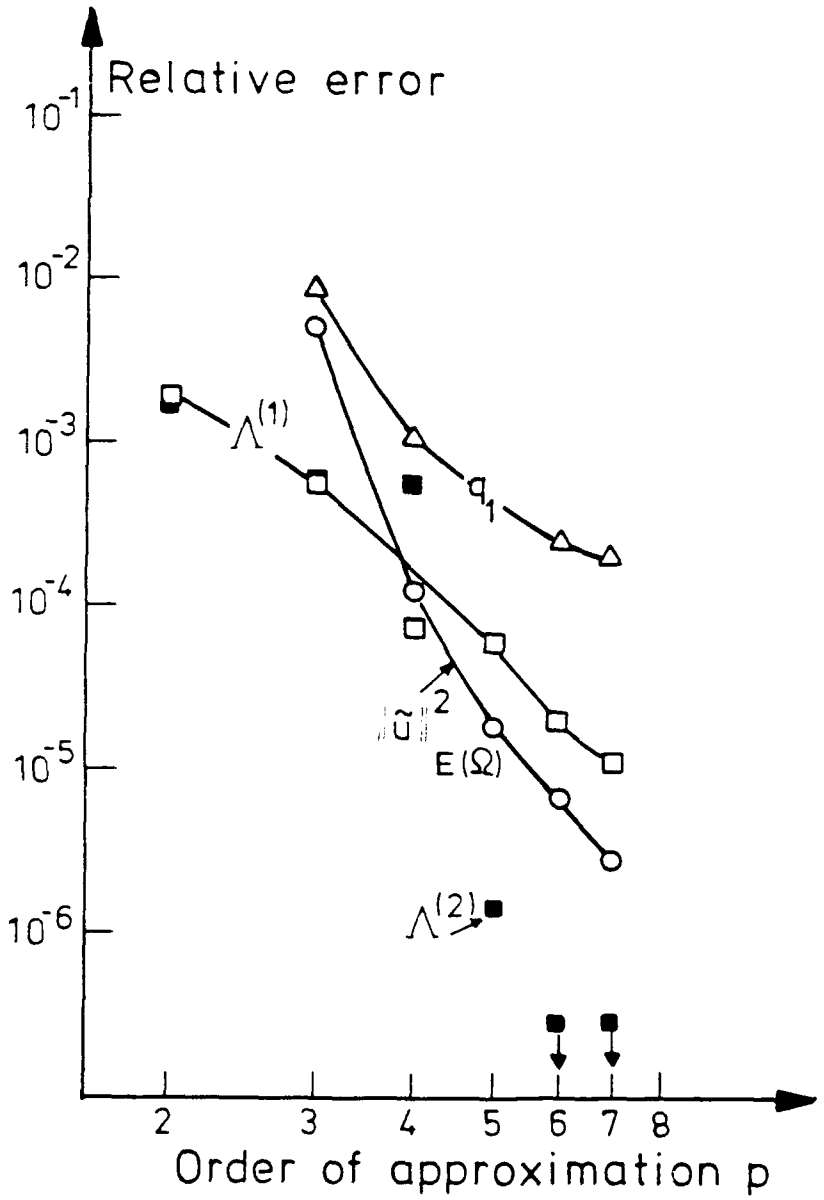

Figure 4: Error in calculated data obtained for benchmark problem with ν=0

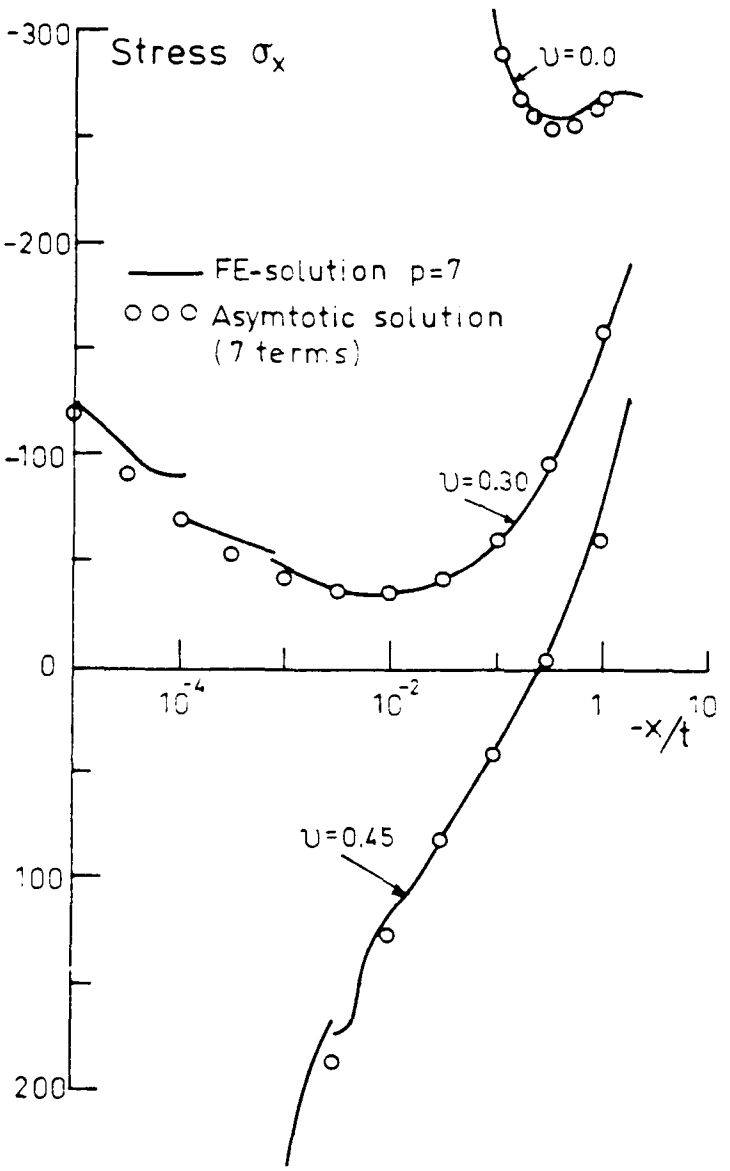

Figure 5: Stress distribution $\sigma_x(x, 0, 0)$ calculated from the asymptotic expansion (8)

Domain	y'	$p=8$	$p=7$	$p=6$	$p=5$	$p=4$	$p=3$	$p=2$
1	0	-1	-1	-6	-24	-9	-225	-421
1	$t/5$	-158	-159	-161	-173	-151	-407	-628
1	$2t/5$	-328	-329	-331	-344	-320	-574	-797
1	$3t/5$	-482	-482	-482	-493	-468	-720	-930
1	$4t/5$	-615	-615	-614	-622	-585	-840	-1026
1	t	-730	-728	-724	-730	-698	-931	-1086
2	0	-730	-729	-723	-732	-691	-936	-1114
2	$6t/5$	-1146	-1145	-1143	-1147	-1148	-1402	-1432
2	$12t/5$	-1331	-1328	-1322	-1320	-1323	-1598	-1648
2	$18t/5$	-1428	-1424	-1415	-1403	-1370	-1622	-1761
2	$24t/5$	-1485	-1481	-1469	-1444	-1384	-1570	-1772
2	$6t$	-1522	-1516	-1499	-1463	-1405	-1541	-1681
3	0	-1522	-1516	-1499	-1461	-1405	-1533	-1675
3	$43t/5$	-1588	-1591	-1599	-1620	-1627	-1571	-1603
3	$86t/5$	-1581	-1578	-1576	-1558	-1593	-1554	-1554
3	$29t/5$	-1569	-1571	-1576	-1566	-1535	-1508	-1527
3	$172t/5$	-1558	-1561	-1554	-1582	-1563	-1458	-1523
3	$43t$	-1561	-1547	-1566	-1531	-1664	-1429	-1541

Table 9: Calculated values of the mode I edge intensity function $K_I^{(1)}(y)$ at six equidistant points inside domains 1 - 3 for $\nu = 0.3$. Plate thickness is t and local y-coordinate inside subdomains is y'

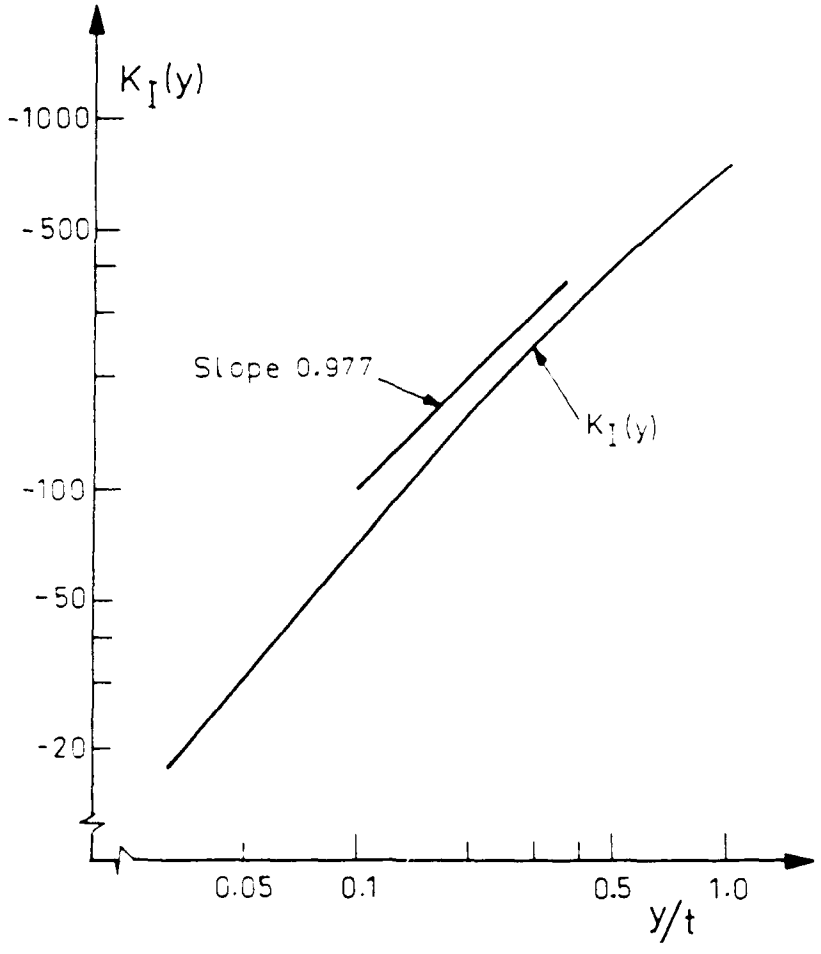

Figure 6: The behaviour of $K_I^{(1)}(y)$ in a neighbourhood of y=0

In figure 7 we depict the pointwise accuracy of $K_I^{(1)}(y)$ for $0 \leq y \leq t$ and the accuracy of the energy. As exact values, the solution for p=8 is used. Once more we find that the accuracy of the computed *pointwise* values of $K_I^{(j)}(y)$ are essentially the same as the accuracy of the global energy.

2.3 The stress concentration problem

In practice the designer tries to avoid sharp (internal) edges and vertices as to prevent fatigue crack initiation. Relevant design parameters for nucleation of such cracks are the magnitude of the local stress components and their time history [2]. The designer has to have an effective tool to get the relationship between stress and radius at a fillet. By using asymptotic analysis (as in the case of the analysis of stresses in a neighbourhood of sharp edges and corners) a rational design formula can be developed.

Consider the solution in a neighbourhood of the radius R_1 (figure 8) and assume for a moment (for reasons of clearity) that the solution is two-dimensional. For a sharp edge, i.e. $R_1 = 0$, the solution may, for any $s \geq 1$ and $s \neq Re[\lambda_\alpha^{(j)}]$, be written

$$\begin{bmatrix} u(r,\theta) \\ v(r,\theta) \\ w(r,\theta) \end{bmatrix} = \sum_{Re[\lambda_\alpha^{(j)}] \leq s} K_\alpha^{(j)} r^{\lambda_\alpha^{(j)}} \Psi_\alpha^{(j)}(\theta) + \text{smoother term} \qquad (11)$$

where $r^{\lambda_\alpha^{(j)}} \Psi_\alpha^{(j)}(\theta)$ are the singular functions of two-dimensional elasticity and the Laplace equation. $K_\alpha^{(j)}$ are constants.

We are interested in solutions for $R_1 > 0$ in a small region (of size $2R_1$, say) around the (rounded) edge EF. We first give the asymptotic behaviour of the displacements for R_1 tending to 0.

These displacements are characterized by the functions $u_{1,\alpha}^{(j)}(x,z)$ defined on an infinite two-dimensional domain with a rounded vertex with radius $R = 1$ (figure 9 with $r \to \infty$ and $\omega = \pi/2$). Denote by $\tau_{kl,\alpha}^{(j)}(x,z)$ the stresses corresponding to the displacements $u_{1,\alpha}^{(j)}(x,z)$. The functions $u_{1,\alpha}^{(j)}(x,z)$ are solutions to the equations of two-dimensional elasticity with boundary conditions that displacements are of the type $r^{\lambda_\alpha^{(j)}} \Psi_\alpha^{(j)}(\theta)$ for r large.

The stresses at a point (x,z) in a neighbourhood of the radius R_1 may then be written

$$\sigma_{kl}(x,z) = \sum_{Re[\lambda_\alpha^{(j)}] < 3\mu} K_\alpha^{(j)} \tau_{kl,\alpha}^{(j)}(\tilde{x},\tilde{z}) {R_1}^{\lambda_\alpha^{(j)}-1} + \mathcal{O}({R_1}^{3\mu-1}) \qquad (12)$$

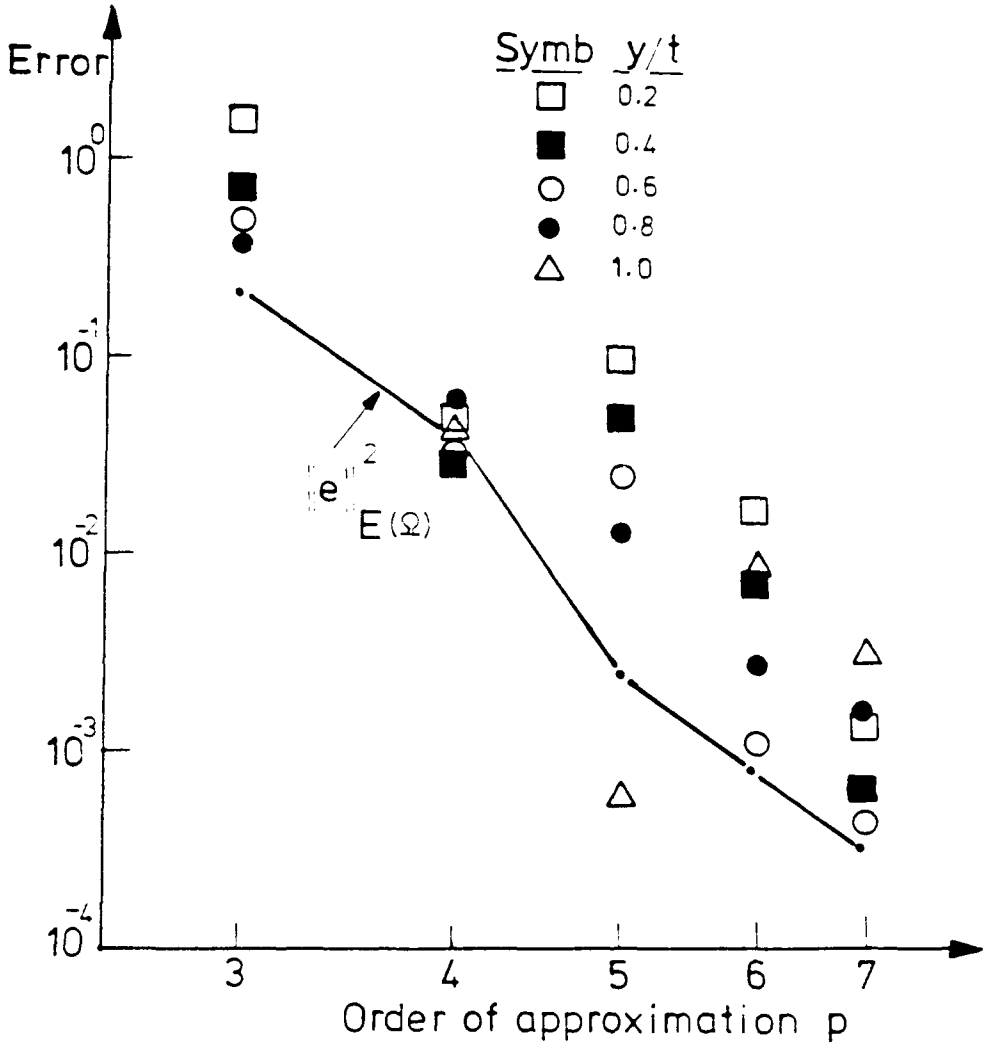

Figure 7: Error in energy $\|e\|^2_{E(\Omega)}$ and pointwise errors of the intensity function $K_I^{(1)}(y)$ for $\nu = 0.3$

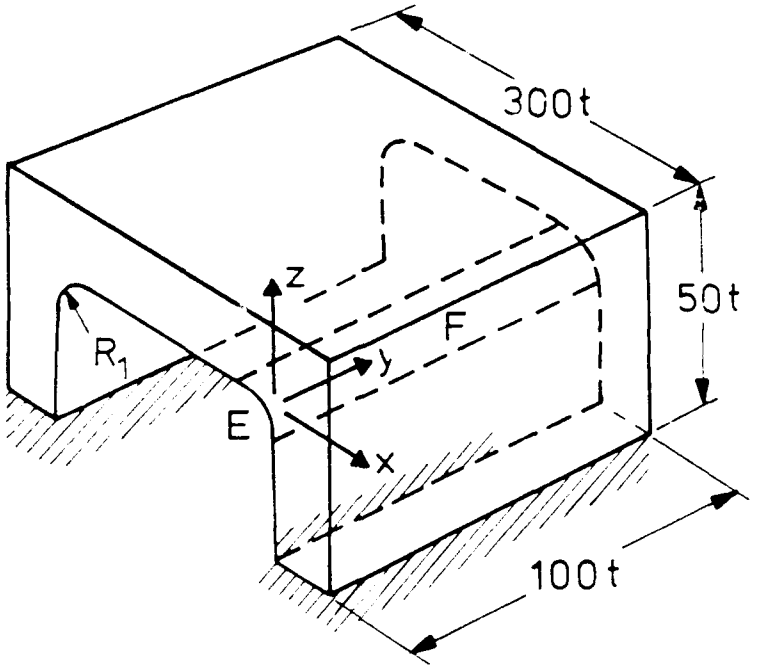

Figure 8: Benchmark problem having radius R_1 at edge EF

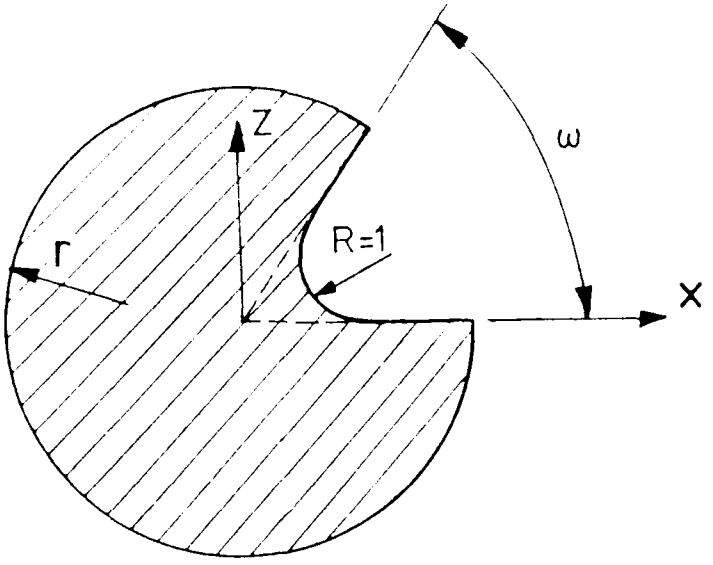

Figure 9: Master domain for calculation of $\tau^{(j)}_{kl,\alpha}(x,z)$

where $\hat{x} = x/R_1$ and $\hat{z} = z/R_1$.

Here $\mu = \min_{j,\alpha} Re[\lambda_\alpha^{(j)}]$ is the singularity exponent with the smallest real part, and (12) gives the asymptotic behaviour for $(\hat{x}, \hat{z})$ fixed and R_1 going to 0 [23]. Therefore we can expect that the sum in (12) gives a good *approximation* for the stress near the rounded edge if R_1 is sufficiently small (i.e. relative to the plate thickness).

For the three-dimensional case, the full mathematical theory is not available. Nevertheless, for R_1 going to 0, we have the following expression for the stresses at a point (x, y, z) close to edge EF

$$\sigma_{kl}(x, y, z) = \sum_{\alpha=I,II,III} K_\alpha^{(1)}(y)\tau_{kl,\alpha}^{(1)}(\hat{x}, \hat{z})R_1^{\lambda_\alpha^{(1)}-1} + \text{higher order terms} \qquad (13)$$

In practice, the functions $\tau_{kl,\alpha}^{(j)}(x, z)$ are determined, once for all, by solving two elasticity problems and the Laplace equation on a two-dimensional domain (figure 9). For three-dimensional problems, we only have to compute the solution on the domain with sharp edges and extract the vertex intensity functions $K_\alpha^{(1)}(y)$. Then we can immediately predict the stresses for small $R_1 > 0$ using (13).

We here give numerical results from an analysis of the folded plate. The case $\nu = 0$ is considered. For $\omega = \pi/2$ we are interested in $K_I^{(1)}(y)$, $K_I^{(2)}(y)$, $K_I^{(3)}(y)$ and $K_{II}^{(1)}(y)$ while the corresponding edge eigenvalues satisfy $\lambda_\alpha^{(j)} < 3\mu$ with $\mu = \lambda_I^{(1)}$.

p	$K_I^{(1)}$	$K_I^{(2)}$ and $K_I^{(3)}$	$K_{II}^{(1)}$
2	-1505.9	$-0.525 \pm 1.278i$	-7.85
3	-1454.3	$-0.368 \pm 2.041i$	-7.19
4	-1482.9	$-2.445 \pm 5.406i$	-7.90
5	-1490.2	$-2.495 \pm 5.456i$	-7.93
6	-1490.8	$-2.511 \pm 5.514i$	-7.91
7	-1491.0	$-2.513 \pm 5.520i$	-7.91
8	-1491.1	$-2.514 \pm 5.524i$	-7.91
9	-1491.1	$-2.514 \pm 5.525i$	-7.91
10	-1491.1	$-2.514 \pm 5.525i$	-7.91

Table 10: Calculated edge functions $K_\alpha^{(j)}$ for $\nu = 0$

Table 10 shows calculated edge intensity functions obtained with a mesh having six cylindrical layers of elements (grading factor 0.15) around edge EF (radius $R_1 = 0$). Table 11 shows the relative error in estimated maximum von Mises effective stress for three different R_1-values. The error is defined as the estimated value (from equation (12)) minus the exact value. As exact solutions we have used FE-solutions obtained with $p = 12$ uniformly on very detailed two-dimensional meshes.

p	$R_1/t = 0.01$	$R_1/t = 0.1$	$R_1/t = 0.25$
2	0.015	0.06	0.11
3	0.020	0.03	0.10
4	0.002	0.05	0.17
5	0.003	0.06	0.17
6	0.004	0.06	0.18
7	0.004	0.06	0.18
8	0.004	0.06	0.18
9	0.004	0.06	0.18
10	0.004	0.06	0.18

Table 11: Maximum relative error in von Mises effective stress at fillet. Maximum effective stresses are 2224, 753, and 480 units for R_1/t= 0.01, 0.1 and 0.25 units respectively

The results in table 11 shows that the estimate (12) is very accurate for R_1 small. The main error of the method in this case is (already for $p > 4$) caused by the term $\mathcal{O}(R^{3\mu-1})$ and not the discretization error. From equation (12) we see that the *relative* error in stress behaves like ${R_1}^{2\mu}$ for R_1 tending to 0. With $\mu = 0.544$ (table 1) we expect that the relative error should behave like ${R_1}^{1.088}$. Data in table 11 show that this is the case.

For the benchmark problem considered, we may simplify (12) somewhat since $K_I^{(1)}$ by far is the largest intensity factor (table 10). By truncating the series (12) to one term the following expression for the maximum von Mises stress at the fillet is obtained,

$$\sigma_{max} = C\,(R/t)^{(\lambda_I^{(1)}-1)} \tag{14}$$

where C=275.

This expression is asymptotically exact for $R \to 0$ (with tree digits accuracy) while for $R/t = 0.01$, $R/t = 0.10$ and $R/t = 0.25$ the relative errors in maximum stress are 0.7%, 4.2% and 7.7% respectively.

A similar approach as shown here for edges can be used for analysis of rounded vertices.

The procedure developed makes it possible to efficiently and reliably compute *pointwise* stresses while the error in edge intensity functions $K_\alpha^{(j)}$ converge as the error in energy. Since (13) is an *analytical* expression for the stresses at the fillet, it is suitable for use in complex dimensioning formulas (fatigue crack initiation etc.). We note that only *one* finite element analysis is needed (with $R = 0$) in order to derive the unknown functions $K_\alpha^{(j)}$ in (13).

3 THE FATIGUE DESIGN OF COMPLEX THREE-DIMENSIONAL COMPONENTS

In this section we demonstrate the reliable analysis of stresses at fillets in a complex aircraft fuselage frame (figure 10) using the techniques reviewed in section 2.

We analyze models having 0.1 - 1.2 million degrees of freedom. Our global finite element model (designed for the h-version of the finite element method) has 5510 elements. The sub-section to be used to demonstrate the reliable analysis of stresses and stress intensity factors using $h-p$ type meshes has 600-800 elements (depending on the goals of the analyses).

We assume that the material is linear isotropic and homogenuous with Poisson's ratio ν=0.3. Traction boundary conditions applied on the sub-section considered are obtained from an analysis of the global model (figure 10a).

3.1 Stresses at hole boundaries

The domain, as in the section 2, has several smooth closed edges (labelled A,B,...). They are similar to the edge AE in figure 1. The main difference is that edges are curved. The curvature of the edges complicates the form (4) for $j > 1$. Additional terms of the type $r^{\lambda_\alpha^{(j)}+k}\Psi_\alpha^{(j,k)}(\theta)$(with k integer and $k \geq 1$) have to be added to (4). For edges $A,\ldots$ we have $\lambda_I^{(1)} = 2.740 + 1.119i$, $\lambda_{II}^{(1)} = 4.808 + 1.464i$ and $\lambda_{III}^{(1)} = 2$. Because $Re(\lambda_\alpha) > 1$, the stresses are essentially smooth and hence the stress intensity functions $K_\alpha^{(j)}(y)$ are not of interest.

Because of assumed boundary conditions (free of tractions in a neighbourhood of the holes), the only nonzero stress at the edge is the normal stress along the edge. If the shape of the edges is analytic then the stresses are analytic functions in the edge length parameter. This function is of special interest since often the stresses have local maxima at the hole boundaries.

We essentially proceed as in section 2 when we computed, in a postprocessing mode, the coefficients of the expansions in the Legendre polynomials (10). In a similar way we can compute stress components σ_{ij} on smooth surfaces by using the double sum

$$\sigma_{ij}(y_1, y_2) \approx \sum_{i=0}^{p}\sum_{j=0}^{p} c_{ij}Q_i(y_1)Q_j(y_2) \tag{15}$$

where y_1 and y_2 are surface coordinates. The advantage of computing the coefficients c_{ij} and using (15) for stress calculation is that the errors in coefficients c_{ij} decrease as the energy error. The problem of computation of stresses along smooth

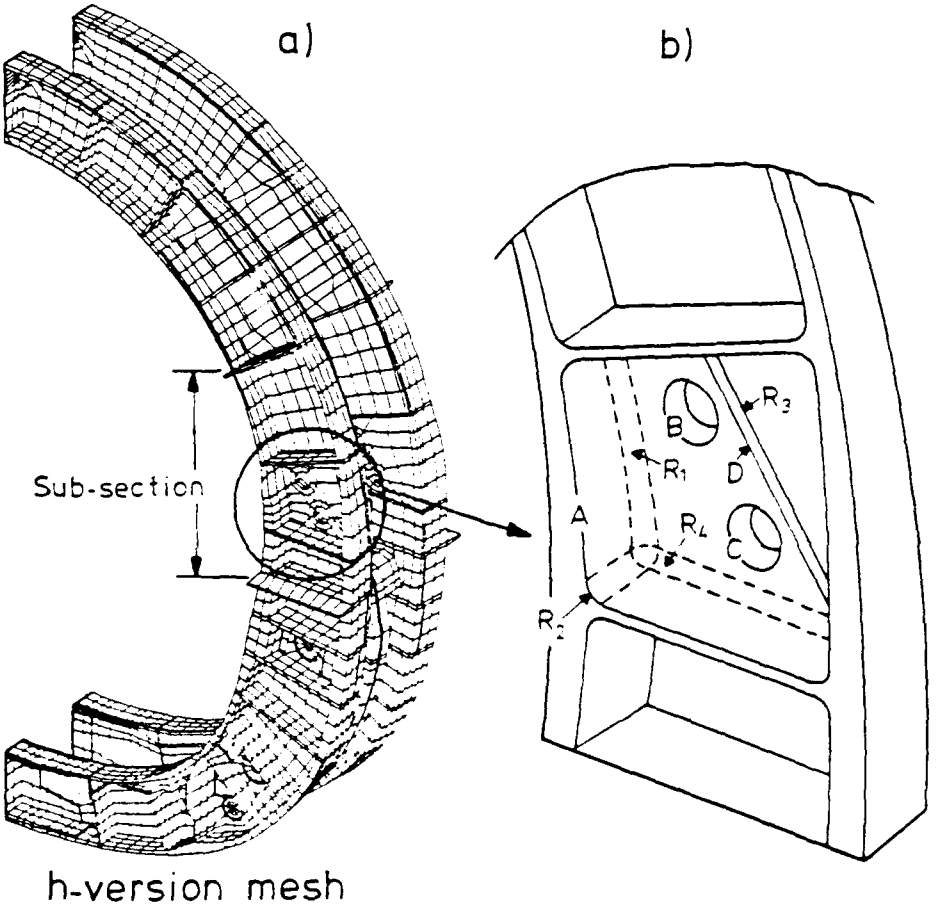

Figure 10: Fuselage frame (a) and sub-section for detailed analysis (b)

edges and on smooth surfaces we address in [23].

3.2 Stresses at fillets

Below we elaborate on some practical aspects of computations of the problem of the fuselage shown in figure 10.

The mesh has to be designed so that the error of the FE-solution decrease exponentially with increasing number of degrees of freedom N in the $p-$range used. We have at our disposition (section 2) postprocessing techniques which allows us to compute engineering parameters of interest, that is stresses, stress intensity factors etc. with the rate of convergence as the energy (not energy norm).

When employing the $h-p$ version of the finite element method, the optimal mesh should be very strongly graded in a proper sense towards the edges and vertices (compare figure 2). With known characteristics of the solution (eg location of boundary layers, strengths of singularities etc.), it is possible using few simple rules for mesh design to obtain high accuracies and an effective control of the error. A mesh generator was implemented in the FE-code STRIPE which uses a coarse mesh (prepared by the user) to create a mesh strongly refined in a neighbourhood of edges and vertices.

Figure 11a shows the coarse user defined FE-mesh ($R_i = 0, i = 1, 2, \ldots 4$) modelling the sub-section of the fuselage (figure 10b). The generated mesh for the $h-p$ version is shown in figure 11b. We have generated additional element layers at internal edges only (where $Re(\lambda_a) < 1$).

Blended function mapping is used [24] to exactly model the shape of the domain (only the polyhedral shape is depicted in figure 11). Note that the details of the generated mesh are invisible at this scale. The input data for the mesh generator is, except the coarse mesh, a list of the edges and vertices where the mesh should be refined and the number of layers of elements to be generated around the vertices and edges. The $h-p$ approach taken has the advantage that the global mesh generation problem splits into a number of local mesh refinement problems. A mesh generator based on these principles is relatively simple to implement.

Figure 12 shows the calculated von Mises effective stress distribution in the frame for p=6. The stress distribution shown is very close (with actual resolution) to the exact solution. The figure shows that for actual radices $R_i = 1/3mm$ analyzed high local stresses at the edges are obtained. The edge labelled R_1 which seems to be most critical will be studied in detail below.

Let us address the problem of determining the smallest radices R_i ($i = 1, 2, \ldots 4$) such that the maximum stress at the stress concentration R_1 , for example, will be the same as the one at the edge B (figure 10b). This is done by the technique

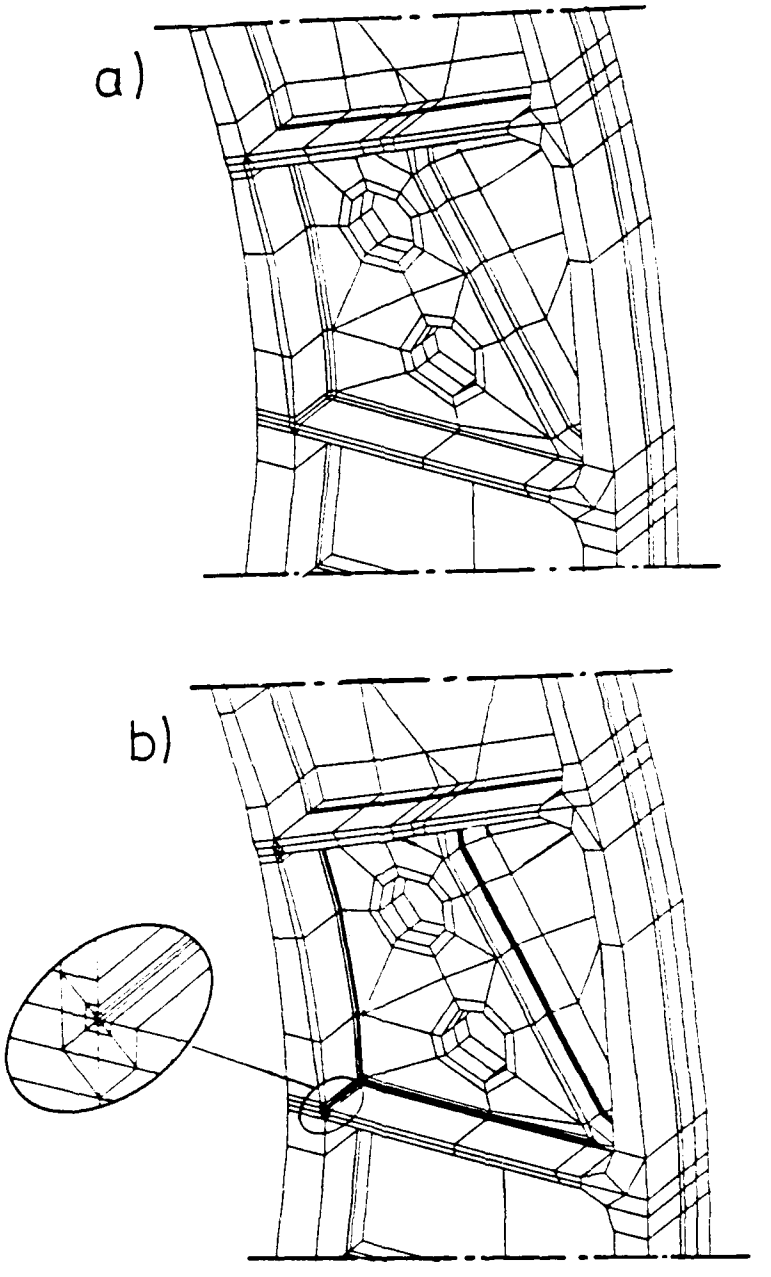

Figure 11: The user-defined coarse mesh (a) and the generated mesh (b)

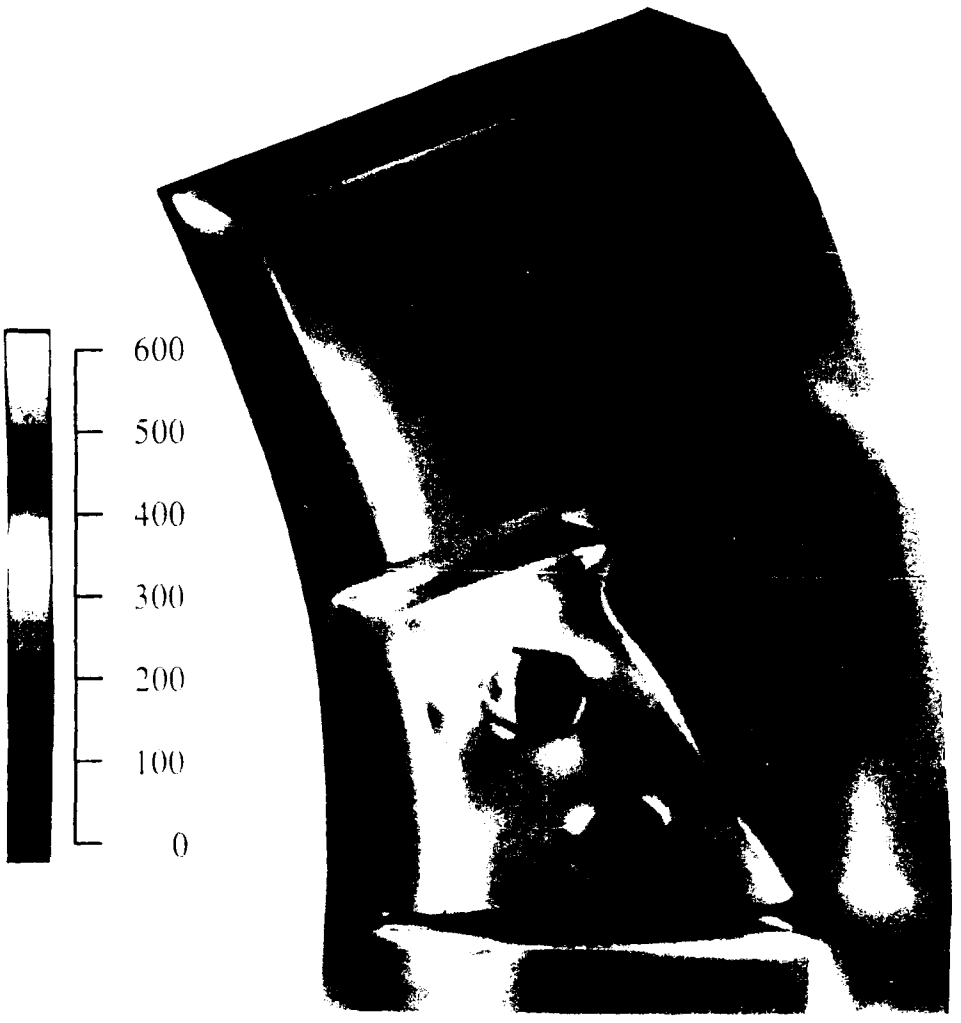

Figure 12: Calculated von Mises effective stress distribution for p=6

described in section 2.3. First we compute the stress intensity functions $K_I^{(1)}(y)$, $K_{II}^{(1)}(y)$ and $K_{III}^{(1)}(y)$ along the unrounded edge and from (13) we compute the stresses.

Calculated edge stress intensity functions $K_\alpha^{(1)}$ for different degrees p of the elements along the edge are shown in figure 13. Three layers of elements have been generated around each edge and vertex (figure 11). Three subdomains along the edge are used for extraction of the polynomial coefficients c_i (10). The results in figure 13 show for p=5 a smooth and continuous variation along the edge. With increasing p the edge intensity functions quickly converge.

Our experience is that by using four layers of elements with the grading factor 0.15, an exponential rate of the convergence is obtained in the range $3 < p < 7$ with approximately the error $\approx C \cdot 10^{-0.6p}$ (for energy, stress intensity factors etc.) provided that the mesh in the entire domain is reasonable. In 3D situations the global mesh often becomes partly distorted or element aspect ratios become very large (for simplicity of input data generation) which may slow down the convergence rate for lower p-levels.

Figure 14 shows the maximum von Mises stress at any point ((x,z)-section) in the fillet as function of the position y along the edge. Stresses have been calculated using (13) and stress intensity data shown in figure 13. For comparison, stresses obtained from a detailed FE-analysis with $p = 6$ (figure 12) with radius $R_1 = 1/3mm$ are shown. Excellent agreement between estimated (13) and calculated local stresses is obtained. Stresses estimated from (13) for different R_1-values are also shown in figure 14. With radius $R_1 = 3.0mm$ the maximum stress in the fillet becomes the same as the maximum stress at the hole boundary (450 Mpa, see figure 12).

To conclude, the use of mesh generation in *a-priori known* areas where solution exhibit strong boundary layers, use of postprocessing techniques to calculate $K_\alpha^{(1)}(y)$ in (13) gives a rational design tool for sizing of fillets in complex three-dimensional components.

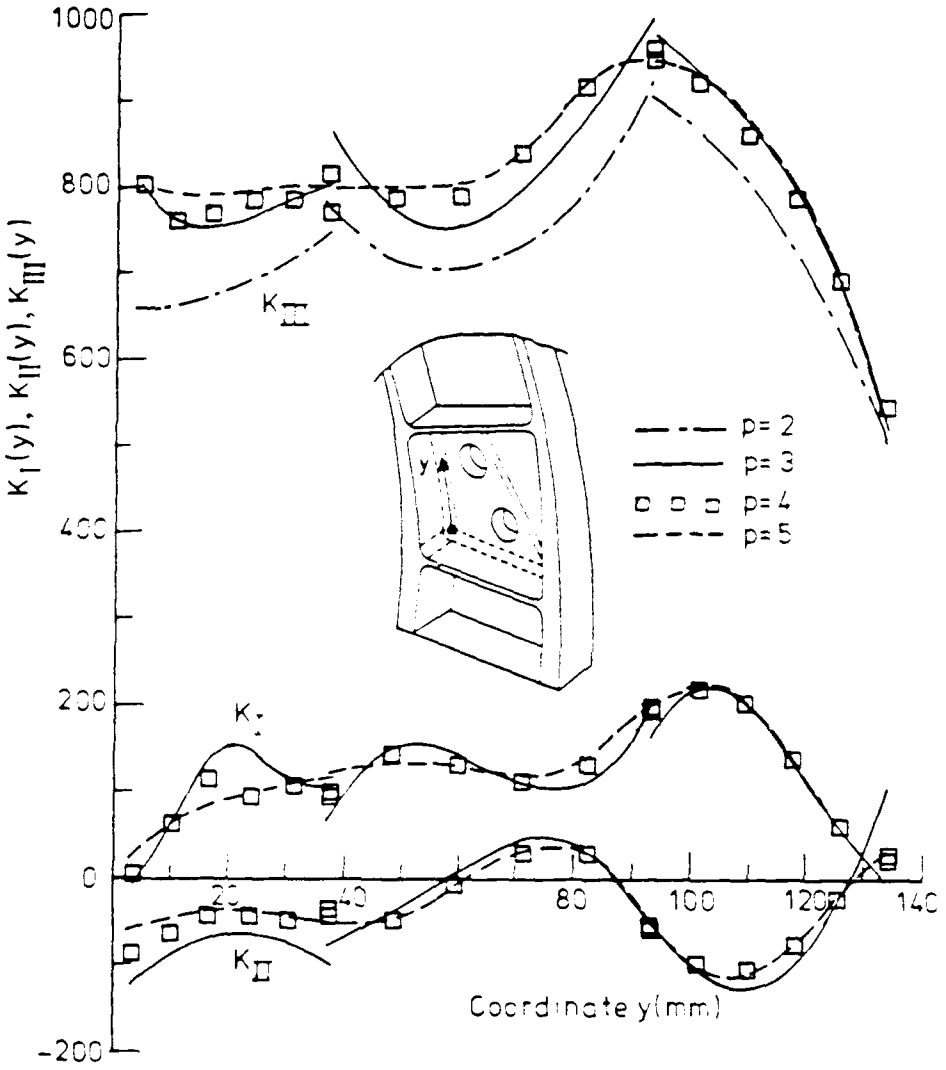

Figure 13: Edge stress intensity functions $K_a^{(p)}(y)$ for different degrees p at critical edge labelled R_1 in frame fuselage

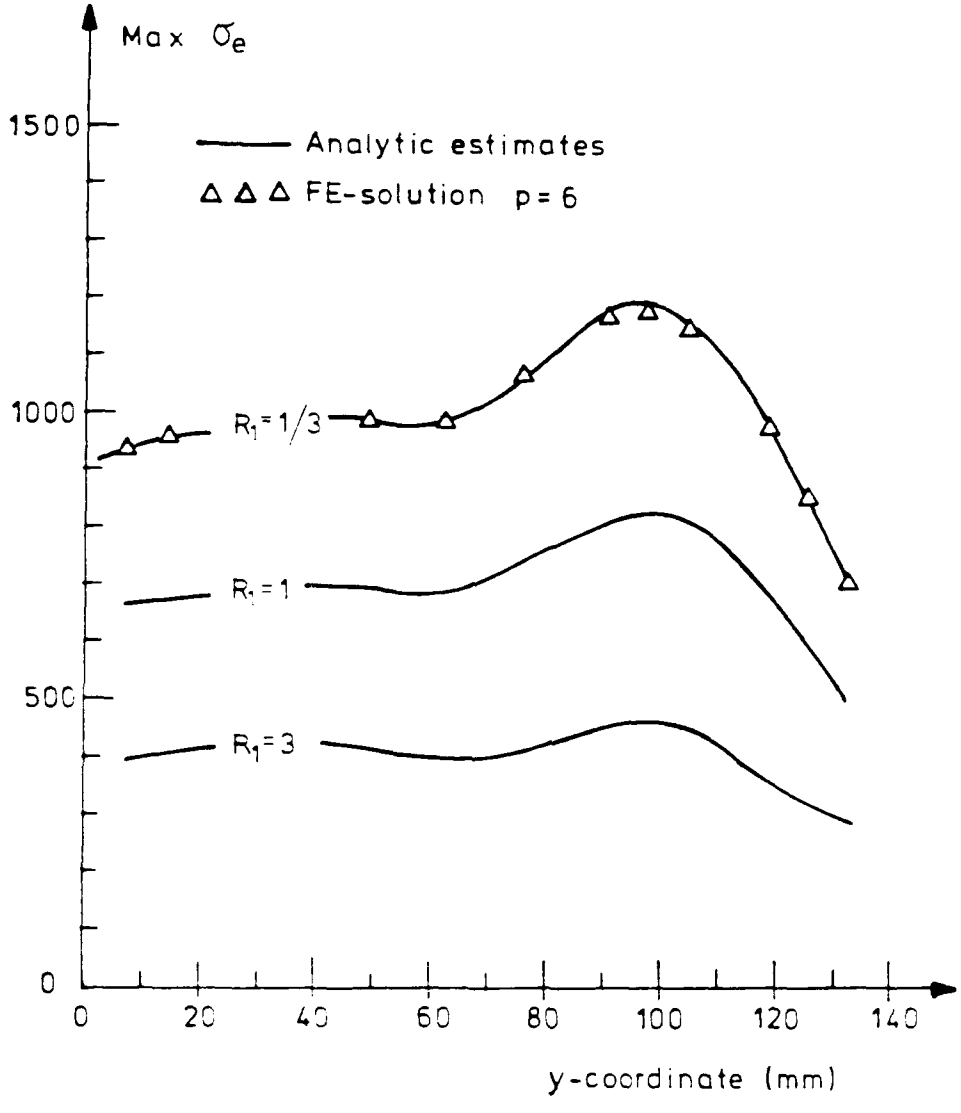

Figure 14: Maximum von Mises stress at critical edge (labelled R_1) with radius R_1

4 THE DAMAGE TOLERANCE ANALYSIS OF COMPLEX THREE-DIMENSIONAL COMPONENTS

Fuselages of the type shown in figure 10 often are designed according to the design code [1]. This code stipulates that *pre-existing* flaws in form of close-fitting cracks of prescribed shape and size and with most unfavorable location and orientation should be considered in the design process. We consider as an example the damage tolerance analysis in case of a flaw located at edge B.

By the principles of section 3 the maximum stresses are determined. The most unfavorable initial crack *orientation* for edge B is such that the plane of the crack is perpendicular to the edge. Based on our knowledge of stresses when no flaws are present (figure 12) we select as the most critical flaw *location* the point of maximum stress at edge B.

The calculated maximum stress σ_1 (MPa) at edge B can be approximated with,

$$\sigma_1 = 450 - 50d \tag{16}$$

where $d < 3mm$ is the distance (mm) perpendicular to the hole boundary (hole radius is $20mm$). The stress gradient over the web thickness is small at the point of maximum stress.

The crack propagation rate (m/load cycle) of a point at the crack front is generally assumed to be a function of the local value of the mode I stress intensity function $K_I^{(1)}$. The growth of the flaw is obtained from integration of crack-propagation "laws" to give the life of the component [2]. In critical cases the designer obviously has to have an effective tool for accurate, efficient and reliable determination of the mode I edge intensity function for different crack dimensions.

4.1 Mesh design

Figure 15 shows a detail of the input data mesh used to calculate the stress intensity functions. The crack front is divided in three sub-intervals. The mesh generator is used to generate four layers of elements close to the crack front. Several different planar cracks with elliptical crack fronts (semi-axes a and b) have been analyzed. The smallest crack size is $a = b = 1.27mm$ [1] and the largest is $a = 3.81mm$, $b = 6.35mm$. Different FE-models corresponding to different crack-sizes are obtained by simply "stretching" the local mesh having a fixed number of elements.

4.2 Calculated edge intensity functions

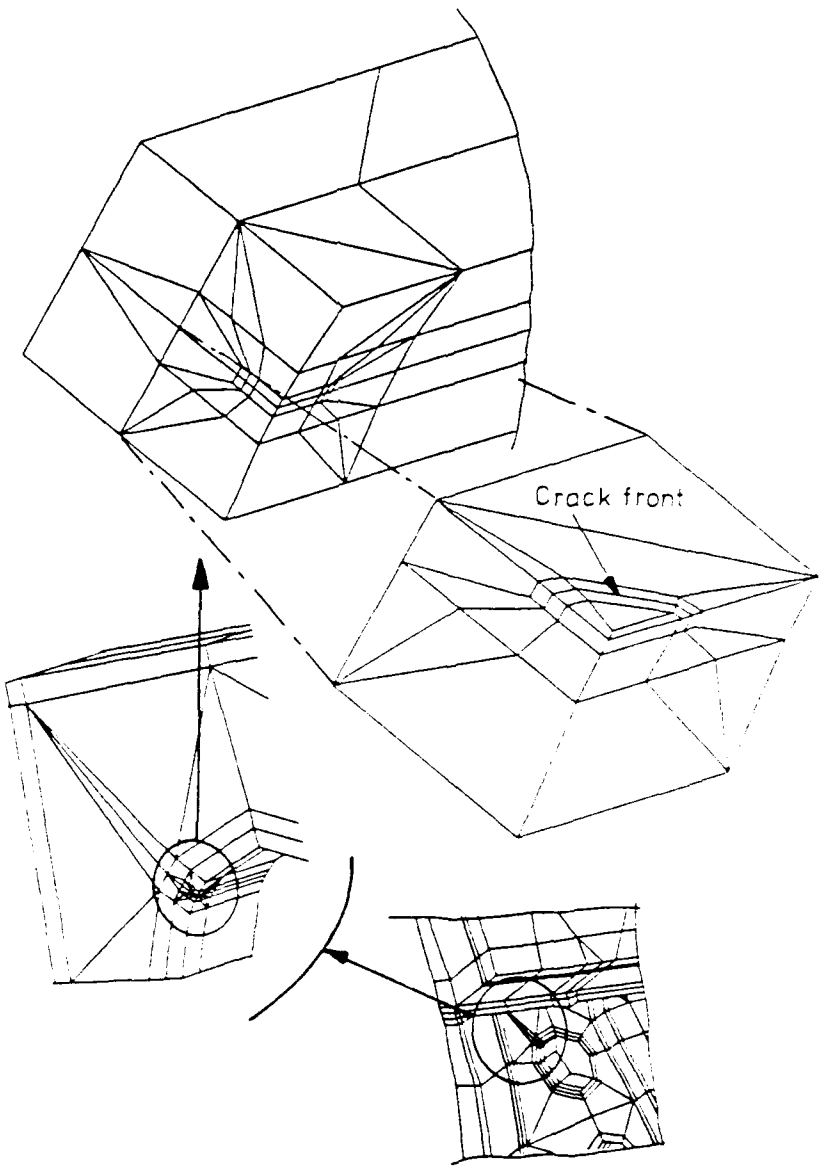

Figure 15: The scheme of the crack and the local mesh used

Domain	x'	y'	$p=6$	$p=5$	$p=4$	$p=3$	$p=2$
1	1.270	0.000	592	596	594	570	527
1	1.268	0.064	597	594	589	567	524
1	1.264	0.128	592	589	582	559	520
1	1.255	0.192	584	582	574	549	514
1	1.244	0.255	579	587	567	542	507
1	1.230	0.318	570	577	559	541	498
2	1.230	0.318	574	572	562	530	509
2	1.135	0.570	564	562	558	540	500
2	0.988	0.797	565	564	560	538	494
2	0.797	0.988	572	569	561	533	490
2	0.570	1.135	585	580	566	537	489
2	0.318	1.230	612	607	594	559	490
3	0.318	1.230	608	612	589	556	494
3	0.255	1.244	620	614	601	563	506
3	0.192	1.255	630	626	612	574	518
3	0.128	1.264	641	636	623	586	529
3	0.064	1.268	650	646	634	598	541
3	0.000	1.270	651	654	645	610	552

Table 12: Calculated $K_I^{(1)}$ at different locations (x',y') on semi-circular crack front $a = b = 1.27mm$

Table 12 shows the calculated (10) edge stress intensity function $K_I^{(1)}$ for a semi-circular crack of size $a = 1.27mm$ and $b = 1.27mm$. We see that for increasing p, the maximum value of $K_I^{(1)}$ converges quickly, smoothly and from below. Our practical experience is that this is the case for reasonable meshes.

We see that the maximum $K_I^{(1)}$ can be computed virtually by *guaranteed* accuracy on models of this (or higher) geometrical complexity.

For very small crack sizes the stress intensity function $K_I^{(1)}$ can be roughly estimated from (16) and weight function data given in handbooks [25]. Such an estimate is based on the assumptions that crack dimensions are negligible as compared to the hole radius and the web thickness. For $a = b = 1.27mm$ the handbook solution is found to overestimate the calculated maximum value ($p = 6$) of $K_I^{(1)}$ with about 10%.

At the two points where the crack front intersects with the traction free surface, $K_I^{(1)}$ should be zero. This follows from (5) and (7) while $\Lambda^{(1)} = 0.5478$ and $\lambda_I^{(1)} = 1/2$. The calculated values of $K_I^{(1)}$ (table 12) though are not zero on the surface! Reason is that the boundary layers are very local. For y small, y being the distance to the vertex, we have

$$K_I^{(j)}(y) = s_{I,1}^{(1)} y^{\gamma_{I,1}^{(j)}}$$

Polynomials of low order (e.g. $p = 6$ and the three sub-intervals used) simply cannot approximate the steep gradient (corresponding to the function $y^{0.078}$) of the edge intensity function close to the two vertices. In case of the folded plate analysed in section 2 the (dominating) gradient was much larger (compare figure 6) and hence easier to recover. If data for the edge stress intensity functions close to the vertex are of interest the vertex-edge intensity factors $s_{I,1}^{(j)}$ can be extracted directly. A procedure is described in [22].

Figure 16 shows the calculated values of $K_I^{(1)}$ as function of p for three elliptical cracks with (very roughly) uniform stress intensities along the crack fronts. The maximum values of the calculated edge intensity functions $K_{II}^{(1)}$ and $K_{III}^{(1)}$ for $a = b = 1.27mm$ are relatively small (about 25 and 10 units respectively).

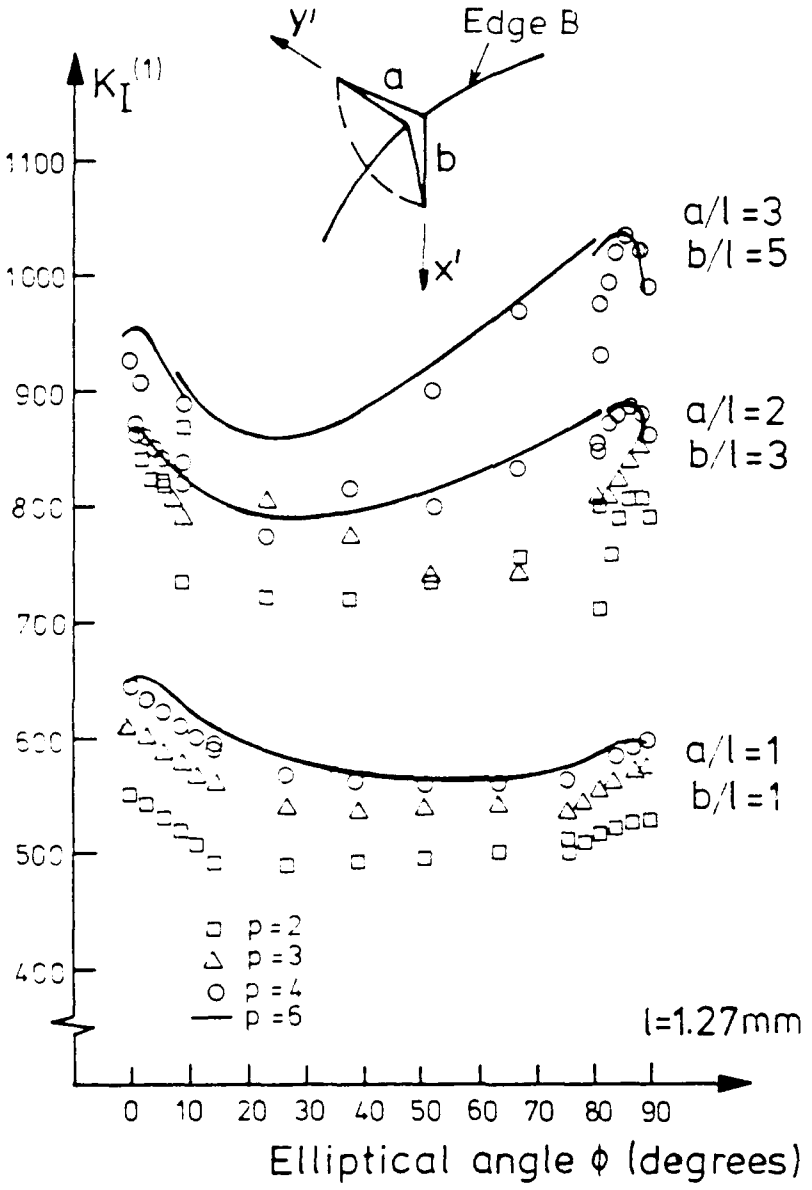

Figure 16: The stress intensity function $K_I^{(1)}$ as function of the degree p and elliptical angle ϕ ($x' = b\cos(\phi)$, $y' = a\sin(\phi)$, $0 \leq \phi \leq \pi/2$)

5 COMPUTATIONAL ASPECTS OF THE $h-p$ VERSION OF FEM

The goal of the $h-p$ version computations presented is to develop a tool for *reliable* and *efficient* determination of any engineering data of interest in complex real-life components.

In the present work this is obtained by using computational procedures which:

- give exponential rates of convergence in the energy norm for accuracies of interest
- use proper postprocessing techniques, which converge as the energy, to calculate design parameters of interest

In previous sections we have addressed these questions on special examples. In this section we will discuss computational aspects of the $h-p$ version of FEM. Instead of analyzing theoretically these questions we will report the basic timing data for the computations of the fuselage parts.

The $h-p$ version when the mesh is properly designed can be understood as the p-version and implemented with uniform increase of the degree p or adaptive increase of p. The proper mesh design for the present approach is obtained using a coarse user-prepared mesh combined with mesh generation at edges and vertices where solution exhibit boundary layers.

The main parts of the analysis are

a) construction of the mesh

b) computation of local and global stiffness matrices

c) solving linear equations

d) postprocessing techniques

If the polynomial orders p of the basis functions are assigned in an adaptive mode there also is.

e) computation of error indicators

Construction of the mesh. This part of the analysis is, in practical cases, the most expensive one. The steady progress of CAD-techniques, improved mesh generators [26] and interfacing programs tend to reduce the cost, though 3D analysis of a complex component is still a major task today.

5.1 Computation of element stiffness matrices

Three-dimensional p-version elements have $\mathcal{O}(p^3)$ degrees of freedom [27] and consequently the element stiffness matrices have $\mathcal{O}(p^6)$ entries. If a standard Gaussian integration scheme with $\mathcal{O}(p^3)$ points is used, the computation of element stiffness matrices require $\mathcal{O}(p^9)$ operations. With such an integration scheme the relative cost of computation of element stiffness matrices will be very significant.

A fast method requiring only $\mathcal{O}(p^6)$ operations is used in STRIPE. The method applies for 3D finite elements of arbitrary shape, arbitrary (practically) Gaussian integration order used, and for linear and nonlinear analysis. The reduction in the number of operations is due to a decomposition of the integration scheme. First $\mathcal{O}(p^3)$ basic 3D integrals are determined using standard Gaussian integration. The $\mathcal{O}(p^6)$ entries in the stiffness matrix are obtained as a linear combination of the basic integrals.

For 3D brick elements, the speedup in Cpu-time obtained as compared to the standard scheme [27] requiring $\mathcal{O}(p^9)$ operations, is a factor 6 to 100 for p=4 to 10 (if $(p+2)^3$ Gaussian integration points are used). With this integration scheme the CPU-times for computation of element stiffness matrices were found to be negligible (1-2 % of total CPU-time) in all cases with uniform p studied here.

5.2 Solving linear equations

Direct methods (as opposed to iterative methods) for solution of the resulting set of linear equations are computationally most efficient (in terms of Cpu-time) for small and medium large problems ($< 10^5$ degrees of freedom, say). Reasons are that in most cases several loading cases (right hand sides) are of importance. For thin shell structures the performance of iterative solvers available are unsatisfactory. The direct solver used in STRIPE is an out-of-core envelope, with domain decomposition ordering.

For practical problems having of the order 10^5 degrees of freedom about 90% of the total CPU-time is spent in the (direct) equation solution phase. This is a similar ratio as for the h-version of FEM.

Table 13 summarizes data for the computational resources needed to analyze the fuselage. CPU-times given include, in cases when a direct solver were used, the analyses for $p = 2, 3, 4 \ldots p_{max}$.

Data given in table 13 apply for one loading case. Increase in CPU-time is a few percent per loading case for the direct solver and about 50% per loading case for the iterative solver. For damage tolerance assessment, several (about 6-10) crack sizes need be analyzed. For the case with the crack at edge B solutions for ten different crack sizes can be obtained with less than a three-fold increase in CPU-time. The

	$K_\alpha^{(1)}$ at edges figure 13	Stresses at fillets figure 14	Crack at edge B figure 15	Entire fuselage figure 10a	Half Fuselage figure 10a
p_{max}	5	6	6	7	8
No of Elements	778	778	610	5510	2755
N (kdofs)	66	103	86	1268	853
CPU-times (hrs)					
.CRAY-XMP/18	2	5	2	-	-
.IBM 6000/550	-	-	5	36	20
Disc (Gbyte)	2	4	2	4	2

Table 13: Model dimensions and computational resources needed to analyze fuselage frame. Direct equation solver was used for models consisting of less than 1000 finite elements

saving in Cpu-time is obtained by using a substructuring technique.

CPU-times reported in table 13 are of the order a few hours for problems having $< 10^5$ degrees of freedom. The error in pointwise stresses, stress intensity factors etc. though are exceptionally small for the p_{max}-levels reported. From a practical point of view a lower p_{max} could have been used. The computational cost is small compared to the cost of preparing the models.

5.3 Super computer performance and large scale problems

The performance of the $h-p$ version will strongly depend on the computer architecture used. Data reported in table 13 apply to a single-processor supercomputer and a powerful work station. The $h-p$ version leads to dense systems of linear equations and a very efficient utilization of the processors. For the work station IBM 6000/RS-550 we obtain speeds of 50-60 MFLOPS independent of problem size. For vectorprocessors (as the CRAY-XMP) the speed increases with the problem size. For the problem having 103000 degrees of freedom the average (for p=2,3,4 and 5) speed is 135 MFLOPS during equation solution on a single processor CRAY-XMP/18. On a 4-processor CRAY-XMP a speedup factor of 3.3 has been measured. Note that these performance figures apply to cases with unstructured meshes leading to exponential convergence rates.

For large problems having of the order 10^6 degrees of freedom the disc storage needed becomes prohibitive if direct solvers are used. The preconditioned conjugate gradient (PCG) method is perhaps the most efficient iterative method for solving structural mechanics problems. The p-version provides in a natural way, a preconditioner (in principle the $p = 1$ approximation) for the conjugate gradi-

ent method. Combined with domain decomposition techniques, powerful iterative solvers for large scale analysis may be developed. The iterative solver [28], [29] was used in the present analyses.

Table 13 briefly summarizes computational resources needed to analyse the complete fuselage. Obviously very complex problems may be reliably solved on powerful work stations.

State of the art parallel computers of today may have hundreds of processors where each individual processor has similar performance as the single processor work station used here. On such computers reliable analyses of entire aircrafts might become feasible. Models of this size and complexity are not needed for reliable computation of local stresses etc. though the concept of using one large model might offer many advantages in an industrial environment.

Postprocessing techniques. The additional cost for computation of stress intensity factors etc. are well below 1% (per loading case) of the time needed to analyze the fuselage parts.

5.4 Computation of error indicators

Results above are all for the case when the polynomial order p is uniformly increased in all elements. The used elemental shape functions are of hierarchical type (i.e. of nodal, edge, face and internal shape functions [27]) which allow the flexible change of the degrees of elements and keep the conformity. Thus, the adaptive selection of element shape functions is possible. Here we report some results when the adaptive scheme is based on the energy norm and the local elemental error indicators characterize the contribution of various shape functions to the energy error. The notation of the degree p_{max} now means the maximal degree of any of the used shape functions.

The cost for calculating the error indicators is significant. If the element stiffness matrices are available, the error indicators can be calculated with a low cost. By using the fast method for computation of stiffness matrices the error indicators can be calculated with a low cost.

As an example we consider the analysis of the stresses at the fillets with the 778 element mesh. Solutions for uniform p=6 and self-adaptive solutions to p_{max}=9 are derived. The adaptive scheme used is described in [30].

The time needed for computation of error indicators and (all) element stiffness data for the self-adaptive p_{max}=9 solution is 10% of the total CPU-time needed. Table 14 gives the energies of the solutions.

We note that the energy convergence with the self-adaptive solution scheme is fast in this case. The adaptive scheme gives, for example, with 25000 degrees of

p	N	$\|\tilde{u}\|^2_{E(\Omega)}$	N	$\|\tilde{u}\|^2_{E(\Omega)}$
2	12480	1.7828	8247	1.7798
3	22068	1.8112	9745	1.8023
4	39675	1.8281	12886	1.8204
5	65676	1.8356	16107	1.8287
6	102894	1.8394	20133	1.8348
7			25166	1.8404
8			31457	1.8461
9			39321	1.8519

Table 14: Energies in solutions for 778-element model analyzed using uniform p-extensions and p-adaptive extensions. Data given are scaled with a factor 10^{-6}

freedom an energy error which is smaller than that obtained for the uniform $p = 6$ solution which has 103000 degrees of freedom. Further, the self-adaptive scheme requires approximately less than half the disk space needed for a uniform scheme.

In general the error in energy norm is in itself of less interest but is a good tool for degree selection p if combined with the accuracy checks for data of interest. The CPU-time needed is a more relevant measure of the effectiveness than the number of degrees of freedom used.

In figure 17 we show the calculated von Mises stress at the *two most critical* points as function of the p-level for the cases with uniform and self-adaptive solution schemes. The figure shows that considerable savings in CPU-time might be obtained by using the self-adaptive solution scheme.

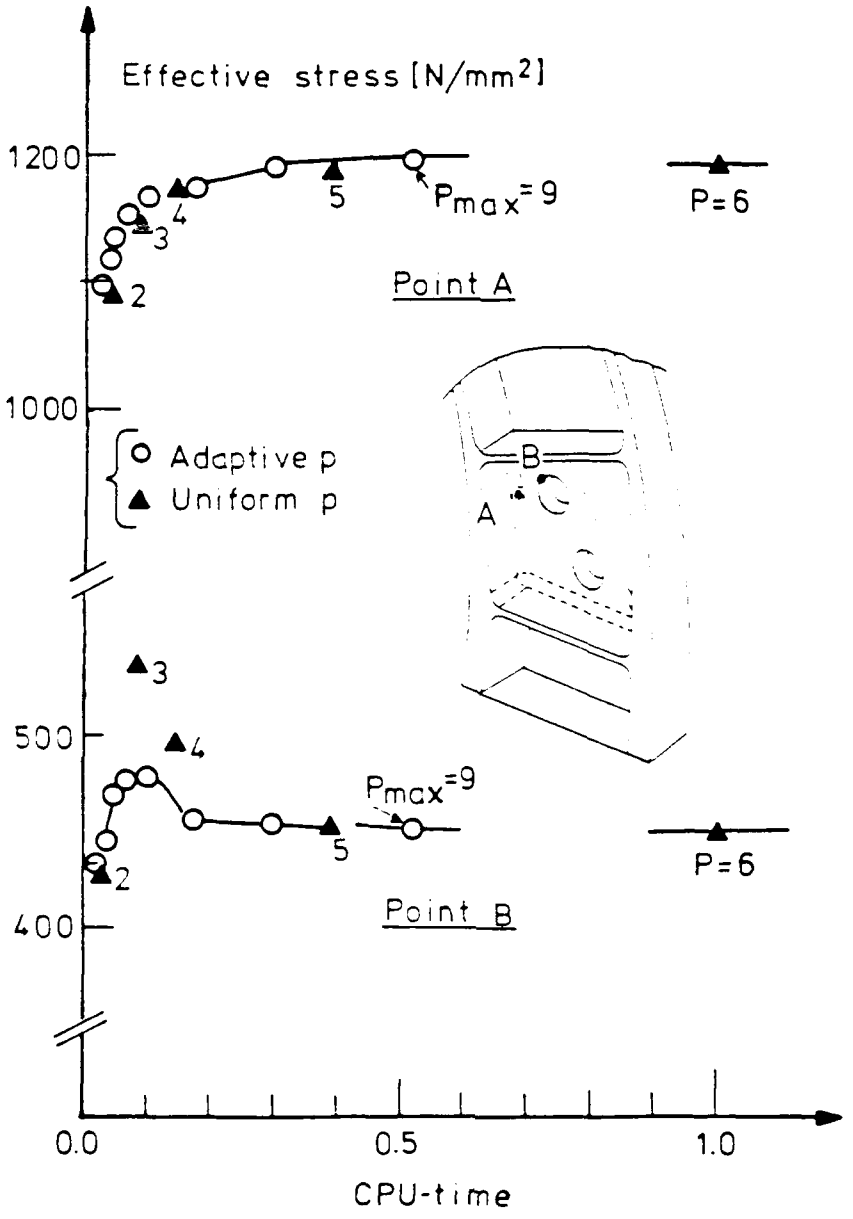

Figure 17: Convergence in pointwise stress at the two most critical points in frame fuselage

6 CONCLUDING REMARKS

We have shown effective approaches for reliable analysis of complex three-dimensional aircraft components with virtually guaranteed accuracy. The main tool was the $h-p$ version of the finite element method combined with new theoretical approaches.

We see that

a) Reliable and accurate accuracy assessment for any computational data of interest, for example the stress intensity factors and functions, stresses etc. is available.

b) The design of the mesh is very different than that for the h-version. The mesh has to be strongly refined. Refinement of a geometrical mesh is recommended. The construction of the mesh relatively simple when some basic rules are obeyed. These rules can relatively easy be implemented in a 3D mesh generator.

c) The used degrees p of the elements are in the range 4-8 and the rate of convergence in any data of interest is exponential in the range of practical accuracy.

d) Computation of local element stiffness matrices could be costly if not properly implemented. If this computation is properly implemented experience show that this part of the analysis requires a small percentage of the entire Cputime.

e) Although the global stiffness matrix is much less sparse than the matrix in the classical h-version, experience shows that the computational cost for an achieved accuracy is still very favourable compared with the classical h-version. When a *reliable* and accurate accuracy assessment of *any data* of interest is required or when high accuracy is needed the $h-p$ version is the only practical alternative.

f) A direct equation solution technique is preferable for problems having up to 50000 to 100000 degrees of freedom especially when several right hand sides (loads) are present. Powerful iterative solvers which are based on the p-version techniques and the PCG-method may be used to efficiently solve complex problems having several million degrees of freedom on todays supercomputers.

g) New methods for the computation of the stress intensity functions and factors and stress concentration factors were proposed, thoroughly analysed and implemented. The rate of convergence is as the rate of the energy, i.e. as the square of the convergence rate of the error measured in energy norm. In the following papers [5],[6],[7], [8],[9],[10] we elaborate in detail on these approaches.

7 REFERENCES

[1] US Air Force. Airplane damage tolerance requirements MIL-A-83444 (USAF). 1974.

[2] S. Suresh. *Fatigue of Materials.* Cambridge University Press, 1991.

[3] C. Mestenyi, A. Miller, and W. Scymczak. FEARS: Details of mathemathical formulation UNIVAC 1100. Technical report BN-994, University of Maryland, 1982.

[4] R. E. Bank. PLTMG: A software package for solving elliptical partial differential equations. Users Guide 6.0, SIAM Philadelphia, 1990.

[5] B. Andersson, I. Babuška, and T. Petersdorff. Computation of vertex singularities and intensity factors for Laplace equation. (to appear), 1992.

[6] I. Babuška, T. Petersdorff, and B. Andersson. Numerical treatment of vertex singularities and intensity factors for mixed boundary value problems for Laplace equation. (to appear), 1992.

[7] I. Babuška, T. Petersdorff, and B. Andersson. Numerical treatment of vertex singularities and intensity factors for elasticity equations. (to appear), 1993.

[8] B. Andersson, I. Babuška, and T. Petersdorff. Computation of vertex singularities and intensity factors for equations of three-dimensional elasticity. (to appear), 1992.

[9] I. Babuška, T. Petersdorff, and B. Andersson. Computation of edge stress intensity functions for Laplace equation. (to appear), 1993.

[10] I. Babuška, T. Petersdorff, and B. Andersson. Computation of edge stress intensity functions for equations of three-dimensional elasticity. (to appear), 1993.

[11] K-J. Bathe, N. S. Lee, and M. L. Buchalem. On the use of hierarchical models in engineering analysis. In *Proceedings of the Workshop on Reliability in Computational Mechanics*, pages 1–1, 1990.

[12] I. Babuška. The problem of modeling the elastomechanics in engineering. *Computer Methods in Applied Mechanics and Engineering*, 82:155–182, 1990.

[13] T. v Petersdorff. *Randwertprobleme der Elastizitätstheorie für Polyedersingularitäten und Approximation mit Randelementmethoden.* PhD thesis, Technical University of Darmstadt, Germany, 1989.

[14] M. L. Williams. Stress singularities resulting from various boundary conditions in angular corners of plates in extension. *J. Applied Mechanics*, 19:526–528, 1952.

[15] V. Z. Parton and P. I. Perlin. *Mathematical Methods of the Theory of Elasticity.* Mir, 1984.

[16] M. R. Dorr. The approximation theory for the p-version of the finite element method. *SIAM J. on Numerical Analysis*, 21:1181–1207, 1984.

[17] M. R. Dorr. The approximation of solutions of elliptical boundary value problems via the p-version of the finite element method. *SIAM J. on Numerical Analysis*, 23:58–77, 1986.

[18] B. Guo and I. Babuška. The h-p version of the finite element method, part 1: The basic approximation results. *Computational Mechanics*, 1:21–41, 1986.

[19] B. Guo and I. Babuška. The h-p version of the finite element method, part 2: General results and applications. *Computational Mechanics*, 1:203–220, 1986.

[20] W. Gui and I. Babuška. The h,p and h-p versions of the finite element method in 1 dimension, part 1: The error analysis of the p-version. *Numerische Mathematik*, 49:577–612, 1986.

[21] W. Gui and I. Babuška. The h,p and h-p versions of the finite element method in 1 dimension, part 2: The error analysis of the h- and h-p version. *Numerische Mathematik*, 49:613–657, 1986.

[22] B. Andersson, I. Babuška, and U. Falk. Accurate and reliable determination of edge and vertex stress intensity factors in three-dimensional elastomechanics. In *ICAS-90-4.9.2. Proceedings of 17th Congress of the International Council of the Aeronautical Sciences*, pages 1730–1746, 1990.

[23] I. Babuška, T. Petersdorff, and B. Andersson. Asymptotics of solutions of boundary value problems at rounded corners. (to appear), 1993.

[24] W. J. Gordon and Ch. A. Hall. Transfinite element methods: Blending function interpolation over arbitrary curved element domains. *Int. J. Num. Meth. Eng.*, 21:109–129, 1973.

[25] Y. Murakami. *Stress Intensity Factors Handbook.* Pergamon Press, 1982.

[26] M. S. Shephard and M. K. Georges. Automatic three-dimensional mesh generation by the finite octree technique. *Int. J. Num. Meth. Eng.*, 32:709–739, 1991.

[27] B. Szabo and I. Babuška. *Finite Element Analysis.* J Wiley SONS, 1991.

[28] J. Mandel. Iterative solvers for p-version finite elements in three dimensions. Prepared for the proceedings of ICOSAHOM 92, Montpellier, France, June 1992, 1992.

[29] J. Mandel. Adaptive iterative solvers in finite elements. In Manolis Papadrakakis, editor, *Solving Large Scale Problems in Mechanics: Development and Application of Computational Solution Methods.* John Wiley and Sons, Ltd, Chichest,England, 1992.

[30] B. Andersson and U. Falk. Self-adaptive analysis of three-dimensional structures using a p-version of finite element method. Report FFA TN 1987-31, The Aeronautical Research Institute of Sweden, 1987.

Issuing organisation	Document No.		
The Aeronautical Research Institute of Sweden (FFA) P.O. Box 11021 S-161 11 BROMMA, Sweden	FFA TN 1992- 17		
	Date Aug 1992	Security Unclassified	Copy No.
	Reg. No.	No. of pages 50	
Sponsoring agency The Defence Materiel Administration (FMV) US office of Naval Research, grant N00014-90-J-1030	Project No. HU-3146 HU-3328	Order/contract	

Title

Reliable Stress and Fracture Mechanics Analysis of Complex Aircraft Components using a h-p Version of FEM

Author(s)

Börje Andersson, Ivo Babuska,
Tobias von Petersdorff and Urban Falk

Checked by

Approved by

Martin Svenzon
Head Structures Department

Abstract

We develop effective approaches with which complex three-dimensional components may be analysed with a high and virtually guaranteed accuracy. The main computational tool is a $h-p$ version of FEM practically realised with the p-version program STRIPE having a mesh generator for automatic mesh refinement at edges and vertices. Use of advanced extraction methods and new theoretical approaches give exponential convergence rates for accuracies in all engineering data of interest. New methods for reliable calculation of local stresses and stress intensity data at edges and vertices to be used for fatigue dimensioning at fillets, damage tolerance assessment of three-dimensional flaws etc. are given. A complex real-life problem is reliably analysed in order to demonstrate the practical usefulness of the procedures advocated. The technical details are given in forthcoming papers.

Key words

Aircraft, Reliability, FEM h-p version, Fracture Mechanics, Stress calculation, a-posteriori, error estimation, STRIPE

Distribution

Copy No.	FMV/FFL	Saab/Scania/L	KTH/ILK	Univ of Maryland	FFA
	1-3	4-6	7	8-75	76-180